Flux regulation through glycolysis and respiration is balanced by inositol pyrophosphates in yeast

Cell

Flux regulation through glycolysis and respiration is balanced by inositol pyrophosphates in yeast

Graphical abstract

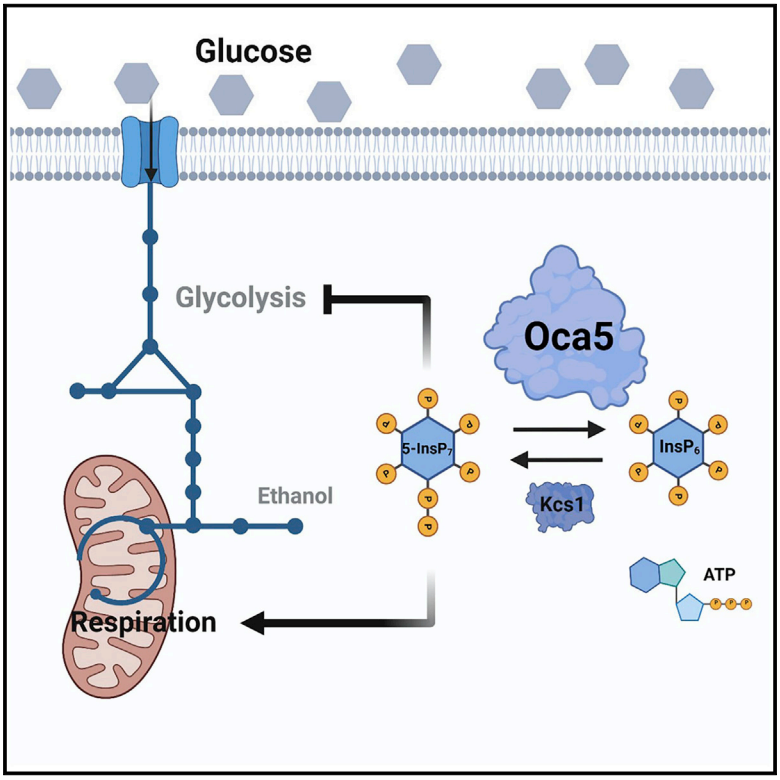

Authors

Ning Qin, Lingyun Li, Xu Ji, ..., Tianwei Tan, Zihe Liu, Jens Nielsen

Correspondence

zihe@mail.buct.edu.cn (Z.L.), nielsenj@chalmers.se (J.N.)

In brief

Glycolysis is considered as the only energy-generating glucose catabolic pathway in eukaryotes. Qin et al. establish a hybrid-glycolysis yeast that disrupts the Embden-Meyerhof-Parnas glycolysis pathway and introduced components of the phosphoketolase pathway. They further identify Oca5 as an inositol pyrophosphatase controlling the balance between glycolysis and respiration activities.

Highlights

- Hybrid of glycolysis with the phosphoketolase pathway made an efficient cell factory
- Oca5, identified as an inositol pyrophosphatase, degrading 5-InsP$_7$ to InsP$_6$
- InsPs control gene expression involved in glycolysis and respiration to balance fluxes
- The mechanism of Oca5 regulating glycolysis and respiration was elaborated

Qin et al., 2023, Cell *186*, 748–763
February 16, 2023
https://doi.org/10.1016/j.cell.2023.01.014

CellPress

CellPress
OPEN ACCESS

Cell

Article

Flux regulation through glycolysis and respiration is balanced by inositol pyrophosphates in yeast

Ning Qin,[1,2] Lingyun Li,[1,2] Xu Ji,[1] Rui Pereira,[2] Yu Chen,[2] Shile Yin,[1] Chaokun Li,[3] Xiaozhen Wan,[1] Danye Qiu,[4] Junfeng Jiang,[5] Hao Luo,[2] Yueping Zhang,[6] Genlai Dong,[1] Yiming Zhang,[1] Shuobo Shi,[1] Henning J. Jessen,[4,7] Jianye Xia,[5] Yun Chen,[2] Christer Larsson,[2] Tianwei Tan,[1] Zihe Liu,[1,9,*] and Jens Nielsen[1,2,8,*]

[1]College of Life Science and Technology, Beijing Advanced Innovation Center for Soft Matter Science and Engineering, Beijing Key Laboratory of Bioprocess, National Energy R&D Center for Biorefinery, Beijing University of Chemical Technology, 100029 Beijing, China
[2]Department of Biology and Biological Engineering, Chalmers University of Technology, SE412 96 Gothenburg, Sweden
[3]Stem Cells and Metabolism Research Program, Faculty of Medicine, University of Helsinki, 00014 Helsinki, Finland
[4]Institute of Organic Chemistry, University of Freiburg, Albertstr. 21, 79104 Freiburg, Germany
[5]Tianjin Institute of Industrial Biotechnology, Chinese Academy of Sciences, Tianjin, 300308, China
[6]College of Veterinary Medicine, China Agricultural University, Beijing, 100193, China
[7]CIBSS - Centre for Integrative Biological Signalling Studies, University of Freiburg, 79104 Freiburg, Germany
[8]BioInnovation Institute, Ole Maaløes Vej 3, DK2200 Copenhagen N, Denmark
[9]Lead contact
*Correspondence: zihe@mail.buct.edu.cn (Z.L.), nielsenj@chalmers.se (J.N.)
https://doi.org/10.1016/j.cell.2023.01.014

SUMMARY

Although many prokaryotes have glycolysis alternatives, it's considered as the only energy-generating glucose catabolic pathway in eukaryotes. Here, we managed to create a hybrid-glycolysis yeast. Subsequently, we identified an inositol pyrophosphatase encoded by *OCA5* that could regulate glycolysis and respiration by adjusting 5-diphosphoinositol 1,2,3,4,6-pentakisphosphate (5-InsP$_7$) levels. 5-InsP$_7$ levels could regulate the expression of genes involved in glycolysis and respiration, representing a global mechanism that could sense ATP levels and regulate central carbon metabolism. The hybrid-glycolysis yeast did not produce ethanol during growth under excess glucose and could produce 2.68 g/L free fatty acids, which is the highest reported production in shake flask of *Saccharomyces cerevisiae*. This study demonstrated the significance of hybrid-glycolysis yeast and determined Oca5 as an inositol pyrophosphatase controlling the balance between glycolysis and respiration, which may shed light on the role of inositol pyrophosphates in regulating eukaryotic metabolism.

INTRODUCTION

Glycolysis is one of the oldest and most fundamental metabolic pathways in cells. In prokaryotes, a divergent evolution of glucose catabolism has been detected,[1] and 57% of prokaryotes utilize the Embden-Meyerhof-Parnas (EMP) pathway.[2] The remaining prokaryotes utilize the Entner-Doudoroff (ED) pathway (~27%),[3] the phosphoketolase (PK) pathway,[4] and the bifidobacterium shunt.[5] In eukaryotes, there has been convergent evolution in the use of the EMP pathway for the catabolism of glucose.[1,6] Grafting of the EMP pathway has been done in prokaryotes.[7] In *Escherichia coli*, non-oxidative glycolysis was constructed and optimized using adaptive laboratory evolution.[8] Furthermore, an analysis of the promiscuity of enzyme activities was performed to identify the flux distribution in this non-oxidative glycolysis pathway.[9] *E. coli* have the coexistence of both the ED and EMP pathways, whereas almost all eukaryotes only rely on glycolysis for the utilization of glucose and have no coexistence of alternative pathways. Many eukaryotes have evolved to enable a very high glycolytic flux such that energy can be produced mainly (or for some even as the sole source) by aerobic fermentation, e.g., cancer cells that show the Warburg effect and yeast *Saccharomyces cerevisiae* as an important model organism that shows the Crabtree effect. This leads to a fundamental question: can the EMP pathway in *S. cerevisiae* be disrupted and grafted with other pathways? If so, how cellular metabolism adapts to such stress remains unclear.

The essence of central carbon metabolism is to balance fluxes through glycolytic and respiratory processes such that cells are provided the required energy, cofactors, and necessary precursor metabolites required for anabolism.[10] Similar to many other eukaryotes, yeast has evolved several key regulatory pathways to control the metabolism process,[11] such as 5′ AMP-activated protein kinase (AMPK), which acts as a Ser/Thr protein kinase to sense the cellular AMP/ATP ratio[12]; the target of rapamycin (TOR) kinase, which controls nitrogen metabolism and protein

biosynthesis and hereby, cell growth[13]; and 5-diphosphoinositol 1,2,3,4,6-pentakisphosphate (5-InsP$_7$),[14] which can sense ATP concentration,[15] so that it can be considered the "energy sensor" to the cell and could participate in the regulation of respiration and glycolysis.[16] Despite significant progress in our understanding of energy metabolism in eukaryotes, the potential mechanisms via which the cells adjust the flux through glycolysis and respiration in response to environmental conditions remain unclear. For example, it is unclear how the transition between fermentation and respiration in yeast is achieved.[17] Therefore, the grafting of the EMP pathway with an alternative pathway may perturb such regulators and hereby provide insights into the mechanism of cells in the regulation of central carbon metabolism.

In the present study, we report the variability of hybrid-glycolysis yeast and identify Oca5 as an inositol pyrophosphatase that can degrade the "energy sensor," 5-InsP$_7$, into inositol hexakisphosphate (InsP$_6$), which then adjusts fluxes through glycolysis and respiration via Gcr1 pyrophosphorylaiton and the Mig1/Hap4 signaling pathway. We further demonstrated the utility of the hybrid-glycolysis yeast in free fatty acids (FFAs) production and using the engineered strain enabled the achievement of the highest reported titer to date. The results of the present study provide insights into how yeast could survive under energy shortage stress through metabolism plasticity via regulation of different transcription factors (TF).

RESULTS AND DISCUSSION

The phosphoketolase pathway combined with transhydrogenase rescued the growth of glycolysis disrupted yeast

Here, we first evaluated the grafting of the native EMP pathway with alternative major glucose catabolic pathways, including the pentose phosphate (PP), ED, and PK pathways. To block glycolysis, the phosphofructokinase (Pfk) is a good target as this enzyme is regarded as the "gatekeeper" of the EMP pathway.[18] Blocking the activity of this enzyme will only inhibit glycolysis and negligibly disrupt gluconeogenesis or the PP pathway (Figure 1A). When we deleted *PFK1* and *PFK2* resulting in complete elimination of Pfk activity, the strain QL1 could not grow in a glucose minimal medium (Figure 1B), indicating that the PP pathway, as the sole glucose catabolic pathway with no energy generation, could not support yeast growth.

Next, we introduced *edd* and *eda* from *E. coli* into QL1 to establish the ED pathway strain QL2. The QL2 strain could also not recover growth in the presence of glucose (Figure 1B). This is consistent with the finding of a previous report,[19] where the bacterial ED pathway could not replace yeast glycolysis without the functional iron-sulfur cluster enzyme, 6-phosphogluconate dehydratase. Finally, the heterologous PK pathway components, including xylulose-5-phosphate-specific phosphoketolase (*xPK*), from *Leuconostoc mesenteroides*,[20] and phosphotransacetylase (*PTA*), from *Clostridium kluyveri*,[21] were introduced into QL1 to generate the PK pathway strain, QL3. QL3 was observed to grow in the presence of glucose (Figure 1B). However, the maximum specific growth rate (μ_{max}) of this strain was very low, i.e., around 0.013 h^{-1} (Figure 1B). In QL1, each molecule of glucose utilized in the oxidative PP pathway generated two molecules of NADPH. To maintain homeostasis of metabolism, it is necessary to balance the production and consumption of NADPH. If the entire amount of glucose consumed resulted in the production of NADPH (in a ratio of two moles of NADPH per mole of glucose), the normal yeast metabolism would be disrupted. To overcome this imbalance, a bacterial transhydrogenase (*TH*) was expressed that could catalyze the transformation of NADPH to NADH (Figure 1A). Expression of *TH* in strain QL1 resulting in strain QL4 enabled slow growth on glucose (Figure 1B), and an even larger effect was observed when *TH* was introduced into the PK pathway QL3 strain. The resulting strain, QL5, had a significantly higher specific growth rate of 0.082 h^{-1} (Figures 1B and 1E). To validate that the EMP pathway was disrupted and grafted with the PK pathway through the oxidative PP (oxPP) pathway in the QL5 strain (the hybrid-glycolysis yeast), we used 100% 1-^{13}C-labeled glucose to trace the rewired pathway (Figure 1C). In the native EMP pathway, the proportion of M+1 (labeled) and M+0 (unlabeled) of pyruvate (and hence also alanine) should both be 50%, as shown in Figure 1C (EMP pathway). If the carbon flux went into the oxPP pathway and the following PK pathway, ^{13}C labeling in the first carbon atom location of glucose would be released as CO_2. The following generated sugar phosphate intermediates would therefore only be M+0, as shown in Figure 1C (oxPP and PK pathway). Indeed, the labeling results confirmed that in wild type (WT) there was ~50% labeling of both M+0 and M+1 in phosphoenolpyruvate (PEP), 2/3-phosphoglycerate (2PG/3PG), and alanine derived from pyruvate generation, whereas there was almost no M+1 labeling in PEP, 2PG/3PG, and alanine in the QL5 strain (Figure 1C). This result indicated that the carbon flux of the EMP pathway was successfully disrupted and rewired in the hybrid-glycolysis yeast QL5. This was further confirmed by the higher ratio of M+0 glutamate, which was derived from acetyl-CoA. The labeling experiments show that we successfully realized the pathway rewiring from the EMP pathway to the oxPP pathway. To test how much carbon flux went into the non-oxidative PP pathway via fructose-6-phosphate (F6P) in the QL5 strain, the M+1 labeling of R5P/X5P/RL5P was also tested. The results showed that both in the WT or the QL5 strain, the R5P/X5P/RL5P were mainly unlabeled (M+0) (Figure 1C), indicating that in both strains the flux going into the PP pathway was mainly via the oxPP pathway. The decreased ratio of M+1 labeling of R5P/X5P/RL5P also proved that the carbon flux into the oxPP in the QL5 strain was higher than that in the WT. This result indicated that TH enables pulling more flux through the oxPP pathway. Taken together, these results proved that we have successfully constructed a hybrid-glycolysis yeast, grafting the EMP pathway with the PK pathway.

Compared with the growth of the reference strain (WT), which had a maximum specific growth rate of 0.35 h^{-1}, growth was still slow in QL5, and this indicated an imbalance of the flux in the central carbon metabolism (Figure 1E). We therefore exposed QL5 to adaptive laboratory evolution using five parallel lines (Figure 1D). After approximately 400 generations, we analyzed the growth of each flask (Figures 1F and 1G) and found that the μ_{max} of each flask was around 0.2 h^{-1}. Specially, the final OD_{600} of flask QL5-1 was around 7 which was much higher than that in the other flasks (Figure 1G). The μ_{max} of flask

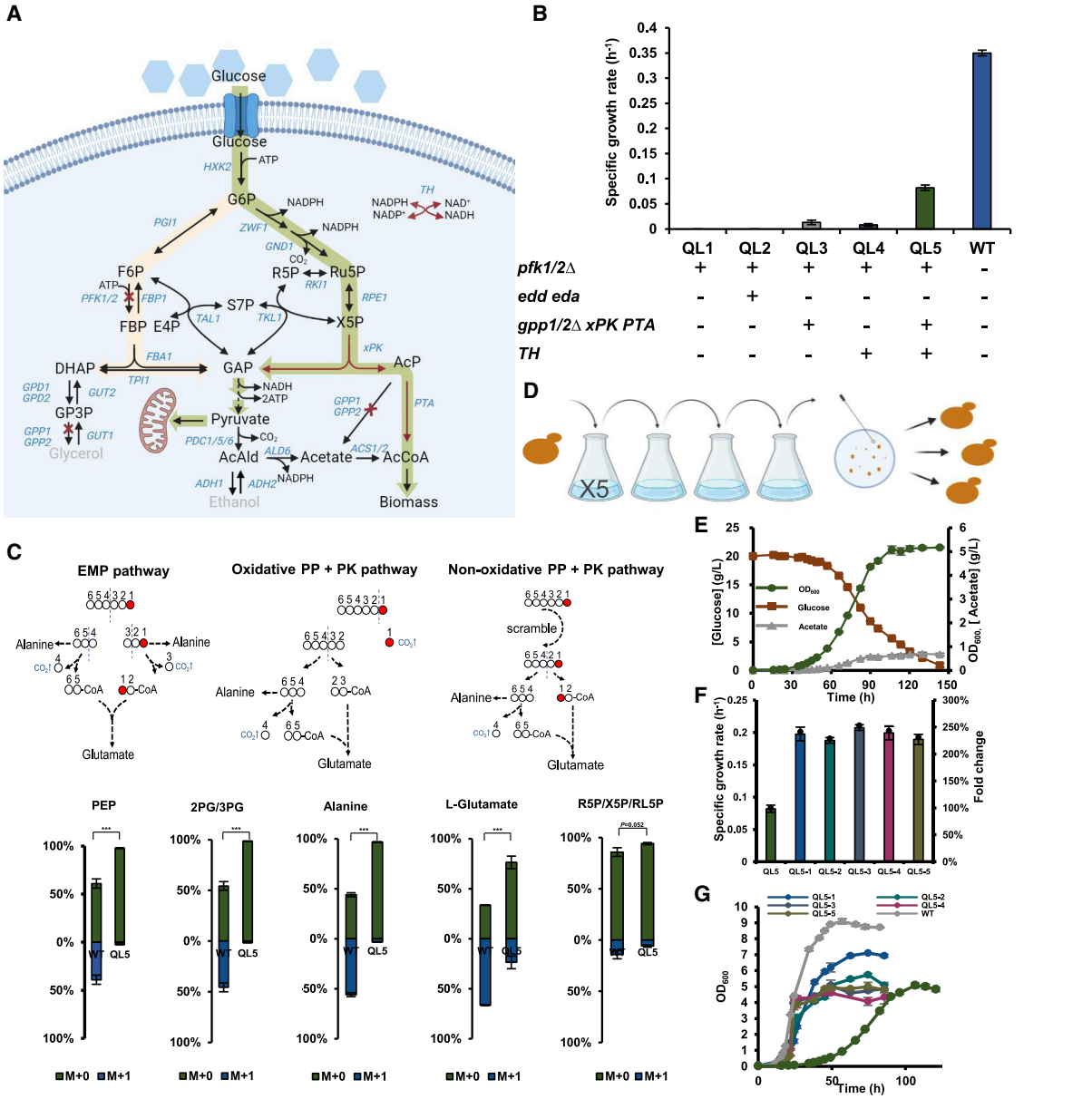

Figure 1. Genetic engineering and adaptive laboratory evolution to obtain a hybrid-glycolysis yeast

(A) Remodeling of the yeast central carbon metabolic network, from native glycolysis (yellow) to the hybrid-glycolysis (green) pathway. The dotted line represents multiple steps, whereas the solid one represents a single step. All introduced genetic modifications are shown in red. Specifically, the red arrow represents the introduction of heterologous genes, and the red cross represents gene deletion. The gray color indicates metabolites not produced during the fermentation of the engineered strains.

(B) μ_{max} of different strains evaluated using the indicated genotype.

(C) The pathway rewiring in the QL5 strain was validated by isotope tracing experiment. 100% 1-^{13}C-labeled glucose was used as the carbon source in the minimal medium. The circles indicated carbon atoms of glucose and the red dot was the 1-^{13}C-labeled carbon atom. Numbers of the sugar phosphate intermediates and glucose refer to the ultimate source of the carbon atoms on the skeleton of glucose. The blue dashed line represents the breakdown of the carbon-carbon bond. The black dashed line represents multistep pathways. The data for the components of isotope tracing experiment list in Table S2.

(D) Adaptive laboratory evolution of QL5 in five independent lines of consecutive shake flasks. At the end of the adaptive evolution experiment, three colonies from each flask were selected for further analysis.

(E) Growth and metabolite profiles of QL5.

(F) μ_{max} of the five parallel lines identified exhibiting improved growth after the evolution experiment.

(G) Growth profiles of the five parallel lines.

Abbreviations are defined in Table S1.

All data are presented as mean ± SD of biological triplicates.

See also Figure S1 and Tables S1 and S2.

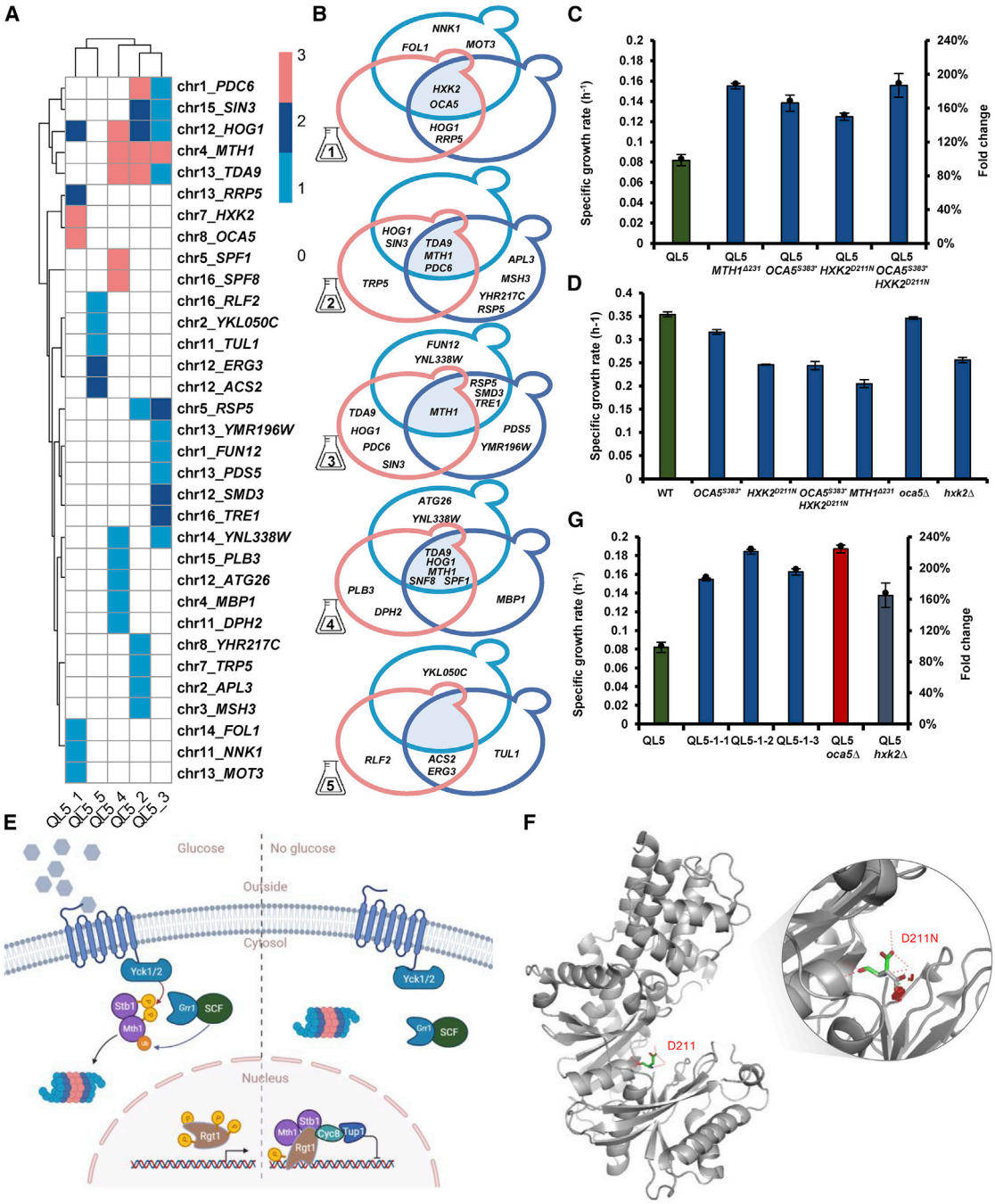

Figure 2. Identification and verification of key driver mutations for growth recovery of the parental strain

(A) Summary of the genome sequencing results of the open reading frame mutations across different lines obtained via adaptive laboratory evolution. The five columns represent the five parallel lines of the evolution experiment. The rows represent mutated genes. The color key represents the number of colonies with these mutations isolated from each flask. The agglomeration method for hclust on the rows and columns was performed using "complete" based on the mutation number of the five parallel lines.

(B) Venn diagrams of the genome sequencing results showing intersections of each evolutionary line. The intersection of each flask indicates dominant mutations across all lines. A detailed description of the mutations can be found in Table S4.

(C) μ_{max} test of reverse engineered strains compared with QL5.

(D) μ_{max} test of introduced mutations in WT.

(E) The Mth1 signaling pathway. In the presence of glucose (left), Yck1/2 are activated by the glucose signal. The activated Yck1/2 then phosphorylates Mth1/Stb1; finally, the phosphorylated Mth1/Stb1 is recognized and ubiquitinated by the SCF and Grr1 complex, subsequently resulting in its degradation by the

(legend continued on next page)

QL5-1 was 0.197 h^{-1}, which was around 2.4-fold higher than that of the parental strain QL5. We selected three colonies from each flask for further analysis (Figure 1D).

Whole genome sequencing and reverse engineering determined the causal relationship between MTH1, HXK2, and OCA5 mutations and cell growth recovery

Following the genomic sequencing and analysis of the 15 isolated clones, it was found that mutations could be roughly clustered into three evolved branches (Figure 2A), including QL5-2, QL5-3, and QL5-4 with the common mutation in *MTH1*, QL5-1 with common mutations in *HXK2* and *OCA5*, and QL5-5 with common mutations in *ACS2* and *ERG3* in two colonies isolated from this flask (Figure 2B). The other colony in QL5-5 exhibited whole genome duplication (Table S4), disturbing the genome sequencing results such that it was not possible to determine the potential driver mutations. Based on the analysis of common mutations from different branches, $MTH1^{\Delta 231}$, $HXK2^{D211N}$, and $OCA5^{S383^*}$ (Table S4) were selected for reverse engineering in the parent strain QL5. The reverse engineering results confirmed that all three mutations recovered cell growth. Specially, the μ_{max} of the strain with the $MTH1^{\Delta 231}$ mutation was 0.155 h^{-1} and that of the strain with the *OCA5* mutation was 0.138 h^{-1}, whereas that of parental QL5 strain was 0.082 h^{-1}. The strain with the $HXK2^{D211N}$ mutation had a μ_{max} of 0.125 h^{-1}, and the μ_{max} of the strain with a combination of the *OCA5* mutation and the *HXK2* mutation was 0.156 h^{-1} (Figure 2C). On the contrary, introduction of this mutation into the WT strain resulted in a decreased cell growth rate (Figure 2D).

When we introduced the $MTH1^{\Delta 231}$ mutation into the WT, the specific glucose uptake rate of the *MTH1* mutation strain was reduced compared with that of the WT (Table S5). Mth1 plays a critical role in the transcriptional regulation of glucose transporters (HXT) in *S. cerevisiae* (Figure 2E), and the sequence analysis of *MTH1* showed that 231 base pairs (133–363) were deleted (Table S4). This mutation omitted the phosphorylation sites 81^{Ser} and 85^{Ser}, which ultimately confer resistance against proteasomal degradation to Mth1.[23] Thus, even in the presence of glucose, the Mth1 mutant could relocate into the nucleus to repress the expression of *HXT* genes, thereby reducing the glucose uptake to balance the overall metabolism (Figure 2E).

Hxk2 is responsible for glucose phosphorylation right after its transportation into the cell by Hxt. When we introduced this $HXK2^{D211N}$ mutation into the WT strain, the specific glucose uptake significantly decreased just like the deletion of *HXK2* (Table S5). These results indicated that the function of $HXK2^{D211N}$ reduced the activity of hexokinase. The crystal structure of Hxk2 in *S. cerevisiae* (Figure 2F)[22] illustrated that the identified 211^{Asp} mutation was located in the catalysis pocket. The side chain of 211^{Asp} forms hydrogen bonds with sugars,[24] and is indispensable for the Hxk2 activity. Simulation of the point mutation in the local structure of Hxk2 illustrated that the original Asp (green) was changed to Asn (gray), which eliminated the ability to form two hydrogen bonds with the substrate and resulted in steric hindrance in the active pocket (Figure 2F). An activity assay of Hxk2 also showed that mutations in 211 almost abolished the activity of Hxk2.[25] Therefore, *HXK2* was also deleted and as for the strain with the mutation $HXK2^{D211N}$, μ_{max} was indeed improved to 1.7-fold compared with that of QL5, i.e., with a μ_{max} of 0.138 h^{-1} (Figure 2G).

The $MTH1^{\Delta 231}$ could reduce glucose uptake and the $HXK2^{D211N}$ mutation restricted the activity of hexokinase. Both mutations restricted the consumption of glucose in QL5 such that it was balanced to the capacity of the downstream pathway, i.e., the heterologous PK pathway. This ensures balancing the levels of cofactors and sugar phosphate intermediates in the central carbon metabolism.

OCA5 regulates glycolysis and respiration

There are only a few reports on Oca5, and its function is unclear. The reverse engineering of $OCA5^{S383^*}$ indicated that the truncated version of Oca5 contributed to the growth recovery of QL5 (Figure 2C). As there were still 397 amino acid residues of Oca5 in the mutant strain, the whole open reading frame of *OCA5* was deleted to gain insights into the Oca5 function. Surprisingly, the deletion strain had significantly improved growth with a μ_{max} of 0.187 h^{-1}, which was even higher than that of the evolved QL5-1-1 and QL5-1-3 strains (Figure 2G).

Compared to the WT, in the bioreactor, the μ_{max} of QL5 was around 0.14 and the deletion of *OCA5* in QL5 resulted in an increase to around 0.2 (Table S5). The specific glucose uptake rate significantly decreased in the QL5 and the QL5 *OCA5* deletion strain, and there was no ethanol or glycerol produced (Table S5). The respiratory quotient (RQ) value of QL5 was around 1.4 whereas in the QL5 *oca5*Δ strain this decreased to around 1 (Table S5). These results indicated that QL5 already had active respiration, but *OCA5* deletion further enhance respiration.

To verify the important role of respiration, we used minimal medium plates with 10 μM of carbonyl cyanide 3-chlorophenylhydrazone (CCCP) (Figure S1A). CCCP is a potent mitochondrial oxidative phosphorylation uncoupler,[26] which uncouples the proton gradient from ATP generation in the electron transport chain. The WT strain could grow on plates with and without CCCP as the EMP pathway could provide ATP under aerobic conditions (Figure S1A). However, the QL5 strain could barely grow on the plates containing CCCP because the energy source was mainly from respiration and the blocked EMP pathway could not generate ATP (Figure 1A). These results demonstrated that the QL5 strain was a hybrid-glycolysis yeast.

proteasome. In the absence of glucose (right), Mth1/Stb1 relocate to the nucleus and, together with Rgt1, Cyc8, and Tup1, bind to the promoters of target genes to block their transcription.

(F) The crystal structure of Hxk2 from *S. cerevisiae* (PDB: 1IG8).[22] The overall structure of Hxk2 is shown in gray in the animation. The 211^{Asp} is depicted as stick-like structure. The dotted line indicates the hydrogen bond of the side chain of 211^{Asp} to other atoms. The amplification of the local structure of D211N, resulting in a mutation from Asp (green) to Asn (gray), is presented using PyMOL. All data are presented as mean ± SD of biological triplicates.

(G) μ_{max} comparison of the three clones from flask QL5-1 with that of *oca5Δ* and *hxk2Δ* strains.

See also Table S4.

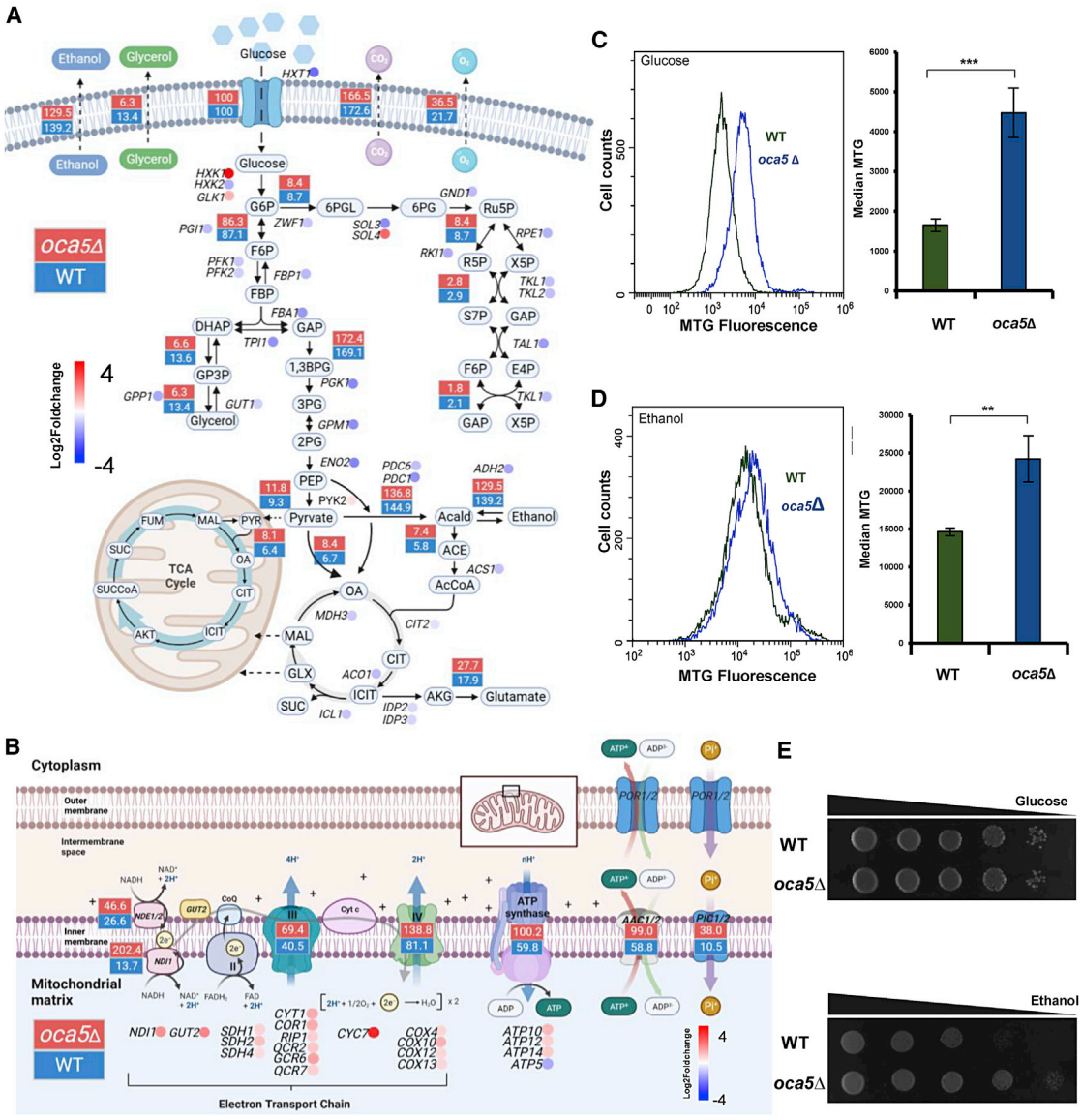

Figure 3. Physiological characterization of *oca5Δ*

(A) Flux balance analysis of WT and *oca5Δ* during the log phase of the batch culture. Fluxes were normalized to 100 units of glucose uptake in central metabolic pathways, and values are shown in the boxes next to the reaction arrows. Results from transcriptional analysis are shown as relative expression levels in *oca5Δ* compared with WT. Gene expression is presented as the $\log_2$ fold change (P-adj <0.05). The $\log_2$ fold change (down/up) of the genes is indicated by blue (down) and red (up) dots.

(B) Fluxes and gene expression for the electron transport chain and ATP synthase displayed similarly to the same fluxes and gene expression as in (A).

(C) Flow cytometric analysis of WT and *oca5*Δ yeast after staining with MitoTracker Green (MTG) during growth on glucose medium. Samples were used during the log phase when the OD_{600} was approximately 1 in the biological triplicates. The bar plots represent the median values of MTG fluorescence intensity in flow cytometric analysis labeling of WT (green bars) and *oca5*Δ (blue bars).

(D) Flow cytometric analysis of WT and *oca5*Δ during growth on ethanol; the sample was derived similarly to that on glucose.

(E) Spotting assay of the WT and the *oca5*Δ strain. The strain was incubated in the minimal medium with 20 g/L glucose or ethanol as a carbon source, and serial dilution was spotted in a plate with a similar medium when the OD_{600} was approximately 1.

Abbreviations are defined in Table S1.

For the flow cytometric analysis, the mean ± SD are from biological quintuplicates. Statistical analysis was performed using two-tailed Student's t test (*$p < 0.05$, **$p < 0.01$, ***$p < 0.001$).

See also Figures S1, S2, S3, S4, and Table S5.

Interestingly, the *OCA5* deletion decreased the ratio of NADPH/NADP$^+$ in the WT strain but had no effect on the QL5 strain (Figure S1B). We suggested this is due to a balancing of the cofactor ratio of NADH/NAD$^+$ and NADPH/NADP$^+$ in the QL5 strain that has *TH* activity (Figure S1B).

To enhance our understanding of Oca5 functions in central carbon metabolism, we evaluated Oca5 mutations in the WT strain, and here we found that the final dry cell weight (DCW) of *oca5Δ* was even 20% higher than that of the WT strain (Table. S5). This result is to some extent impressive, since strains are naturally evolved to gain faster cell growth and higher cell weight. Our result showed that the *oca5Δ* could improve the biomass yield of the WT strain, indicating an improved energy metabolism efficiency. The deletion of *OCA5* in the QL5 and the WT strain both resulted in a higher ATP/ADP ratio, which supports this hypothesis (Figure S1C). On the other hand, either the whole deletion or the mutant version only resulted in a small decrease of 5%–9% in μ_{max} (Table S5). The specific glucose uptake rate did, however, decrease to approximately 86% of the value for the reference strain, which indicated the *oca5*Δ restricted glucose consumption of the strain. Furthermore, ethanol production decreased by 15% and glycerol production decreased by 58%, which indicated that the *oca5*Δ restricted fermentation of the strain. The RQ value decreased to approximately 56% of the value for the reference strain. The specific oxygen uptake rate of the *oca5*Δ strain was also higher than that of the WT strain, which indicated that the *oca5*Δ improved respiration and decreased fermentation at the same time. We also constructed a strain with two copies of *OCA5*, with both copies expressed by the native promoter. Opposed to the *OCA5* deletion, overexpression of *OCA5* resulted in increased ethanol and glycerol production, and RQ value (Table S5). These experiments indicated that Oca5 may function in repressing respiration and stimulating fermentation.

To further characterize the effect of Oca5 on central carbon metabolism, flux balance analysis (FBA) and flux sampling were performed. The absolute metabolic fluxes (Figure S2A) demonstrated that fluxes through glycolysis and the pyruvate dehydrogenase (PDH) bypass during growth on glucose decreased in *oca5Δ* compared to those in the WT, respectively. This indicated that the deletion of *OCA5* resulted in a restriction of the glycolytic flux. Fluxes through all the complexes in the oxidation respiratory chain were increased by approximately 50% of that of the WT strain (Figures S2 and S3). Normalized fluxes illustrated that the carbon fluxes through glycolysis and the PDH bypass in *oca5Δ* were slightly declined from those of WT, whereas there was a significant increase in fluxes through the respiratory chain (Figures 3A and 3B). The electron transport chain (ETC) consists of complex I–VI that together with ATP synthase (complex V) transfers electrons and generates ATP. The FBA and the flux sampling result showed that in the ETC, the flux through Nde1 and Ndi1, which are equivalents of complex I in mammals, and through complex III, complex IV, and complex V significantly increased (p value shown in Table S1) in *oca5Δ* (Figures 3B and S3B), indicating a strong ATP generation by oxidative phosphorylation in *oca5Δ*. This notable difference would lead to a higher overall ATP yield than that of substrate phosphorylation in the WT strain (Figures 3A and 3B), thus yielding a higher biomass yield in *oca5Δ* (Table. S5).

To verify the higher respiratory capacity of *oca5Δ,* a dropping assay with ethanol as the carbon source was performed, and the result showed that *oca5Δ* grew faster than the WT strain (Figure 3E). As a non-fermentable carbon source, ethanol can only be metabolized through mitochondrial respiration, and the dropping assay therefore supports an increased mitochondrial activity in *oca5Δ*. This was also confirmed by flow cytometry analysis of the strain stained by MitoTracker Green (MTG), which showed that the mitochondria in *oca5Δ* accumulated more MTG during growth on both glucose (Figure 3C) and on ethanol (Figure 3D). This result suggested that *oca5Δ* had a higher mitochondrial mass independent of the carbon source.

To reveal the mechanisms underlying how Oca5 regulates glycolysis and respiration in yeast, we performed RNA-seq analysis. The transcriptome analysis identified 1,072 genes with significantly changed expression in *oca5Δ* compared with WT (Figures S4A and S4B). The pathway enrichment analysis (Figure S4C) results showed that the carbon metabolism, glycolysis, ribosome, and biosynthesis of amino acids were downregulated. Meanwhile, oxidative phosphorylation (Figure S4C) was significantly upregulated. In metabolite enrichment analysis (Figure S4D), we identified genes related to ferricytochrome C in the mitochondria that were upregulated, and those associated with glycolytic metabolites were downregulated. These results are consistent with those of the FBA analysis. When analyzing specific genes, we found that genes involved in glycolysis were significantly downregulated (Figure 3A), and genes in the ETC, including ATP synthase, were significantly upregulated (Figure 3B).

Using the hybrid-glycolysis yeast as a platform cell factory

In addition to serving as a model organism, *S. cerevisiae* serves as a cell factory for producing foods, chemicals, fuels, and pharmaceuticals.[27] When engineering yeast for the production of various chemicals, it is generally challenging to prevent ethanol production as a major by-product.[10,28] The hybrid-glycolysis yeast with *OCA5* mutation obtained here exhibited a significant remodeling of the entire central carbon metabolism (Figure 1A), lacking ethanol production in the presence of abundant glucose. This revealed the potential of this hybrid-glycolysis yeast as a platform strain, in particular for the production of acetyl-CoA-derived chemicals. FFAs are used widely in the chemical industry and can also be used as biofuels, but the titer and yield need further enhancement to realize an economically viable process for industrial-scale production.[29] We therefore investigated the production of FFAs to explore the potential of our hybrid-glycolysis yeast as a platform cell factory (Figure 4A).

First, we constructed the FFAs module in the WT strain (Figure 4A), with common optimization targets of FFAs engineered.[30] The resulting FQL2 strain could produce 1,060 mg/L FFAs (Figure 4B). Next, we introduced the FFAs module in the QL5 *oca5*Δ strain, together with reduced expression of *TH* to balance the cofactor pool between cell growth and FFAs production, as well as the mutation of *MED2** to further reduce fermentation.[17] The resultant FQL26 strain could produce FFAs at a much higher level, i.e., 2,188 mg/L, which was 2-fold of the production by FQL2 (Figure S5). Following shifting from the use of

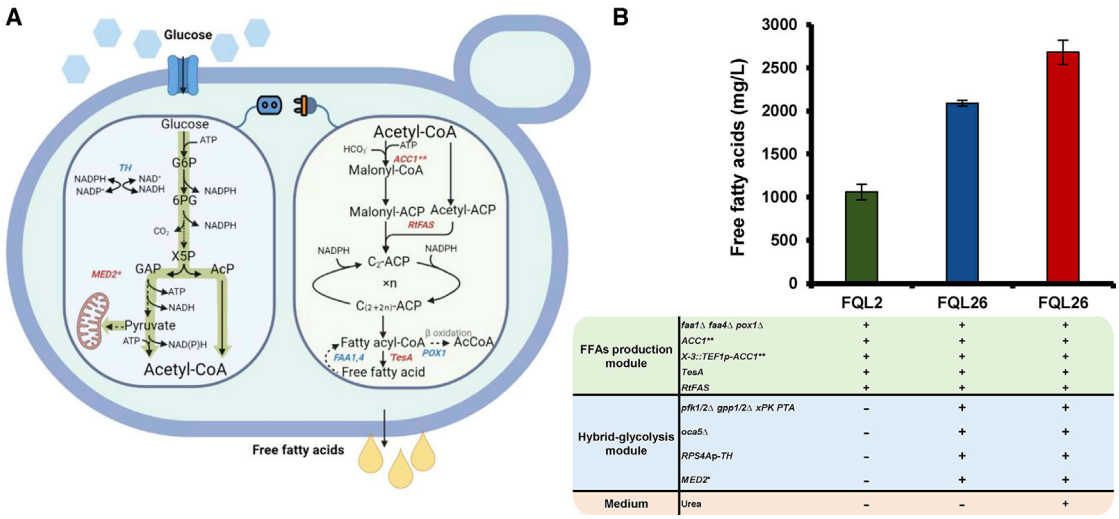

Figure 4. A free fatty acids (FFAs) production module was added to the hybrid-glycolysis strain

(A) The hybrid-glycolysis yeast central carbon metabolism module (blue) was coupled with a FFAs production module (green). Downregulated (or knockout) genes are shown in blue, and upregulated (or mutated) ones are shown in red. The dotted line represents multiple steps, and the solid one represents a single step.

(B) FFAs production of the hybrid-glycolysis yeast (blue). Coupled with the FFAs production module (green), the hybrid-glycolysis yeast could produce up to 2,678.3 mg/L FFAs, which is the highest shake flask production to date.

Abbreviations are defined in Table S1.

All data are mean ± SD of biological triplicates.

See also Figure S5 and Table S6.

7.5 g/L $(NH_4)_2SO_4$ to 2.27 g/L urea as the nitrogen source,[31] FFAs production reached 2,678 mg/L (Figure 4B). This is the highest titer of FFAs that has been reported in *S. cerevisiae* for shake flask fermentations. More importantly, the carbon yield reached 0.134 g FFAs/g glucose, which is the highest reported yield for *S. cerevisiae* under various fermentation conditions (Table S6). A particular advantage of our hybrid-glycolysis yeast for FFAs production is that it does not require fed-batch fermentation; however, simple batch fermentation can be applied, which offers a significant advantage for large-scale production.

Oca5 was identified as an inositol pyrophosphatase in *S. cerevisiae*

To identify the function of Oca5 and reveal the mechanism of the global effect of *OCA5* deletion on central carbon metabolism, we first constructed a phylogenetic tree of Oca5 (Figure 5A). Oca5 was distant from other proteins in the Oca family (Figure 5A), but transcriptional profiles of *OCA1*, *OCA2, OCA3* (*SIW14*), *OCA5*, and *OCA6* deletion strains were highly similar, indicating that these proteins belong to one protein complex,[32] though another study pointed that the OCA family should not include *OCA1*.[33] We therefore deleted *OCA2*, *OCA3*, *OCA4*, and *OCA6* in QL5, and these deletions resulted in an increased growth rate of QL5 by 1.5-fold, 1.8-fold, 1.6-fold, and 2-fold, respectively (Figure 5B). Additionally, the spotting growth assays for the *OCA* gene deletion strains demonstrated that growth on ethanol was faster than that of the WT strain (Figure 5C), which indicated that these *OCA* deletion strains also have stronger respiratory capacity than WT. Similarly, with *OCA5* deletion, *OCA3* deletion, or *OCA3* with *OCA5* double deletion resulted in lower specific glucose uptake rate; ethanol and glycerol production rates; and RQ value (Table S5). These results indicated that *OCA3* and *OCA5* both function in repressing respiration and stimulating fermentation.

High-throughput data on protein interactions imply potential physical interactions between the Oca proteins,[34] but our yeast two-hybrid (Y2H) analysis (Figure S6A) did not show interaction of Oca5 with other Oca proteins, such as Oca3. Although the phylogenetic analysis based on the whole protein sequence indicated that Oca5 is distant from other proteins in the Oca family (Figure 5A), a structural comparison of Oca5 and Oca3 showed that four peptide sections around the active site were very similar (Figures S6B and S6C), indicating that Oca5 may have a similar function as Oca3. Oca3 (Figure 5D) has been identified as an inositol pyrophosphatase,[35] which could specifically catalyze the degradation of phosphoanhydride bonds on the fifth position of 5-$InsP_7$ to form $InsP_6$[15].

To evaluate if Oca5 has a similar function as Oca3, we need 5-$InsP_7$ as a substrate. In *S. cerevisiae*, 5-$InsP_7$ is synthesized from $InsP_6$ in a reaction catalyzed by Kcs1 with the consumption of ATP.[36] The mammalian isoforms of Kcs1 are Ip6k1, Ip6k2, and Ip6k3.[36] Currently, there is no commercially available 5-$InsP_7$, and based on one reported method,[37] we used Ip6k1 from *Mus musculus* to synthesize 5-$InsP_7$ from $InsP_6$ (Figure 5E). Synthesized 5-$InsP_7$ could be separated from $InsP_6$ by 35% polyacrylamide-gel electrophoresis (PAGE) analysis.[38] The generated band was identified by mass spectrometry (MS) as 5-$InsP_7$ (Figures S6D and S6E). Oca5 was then purified and characterized using concentrated 5-$InsP_7$ as the substrate for Oca5. The results showed a change in the mobility of bands

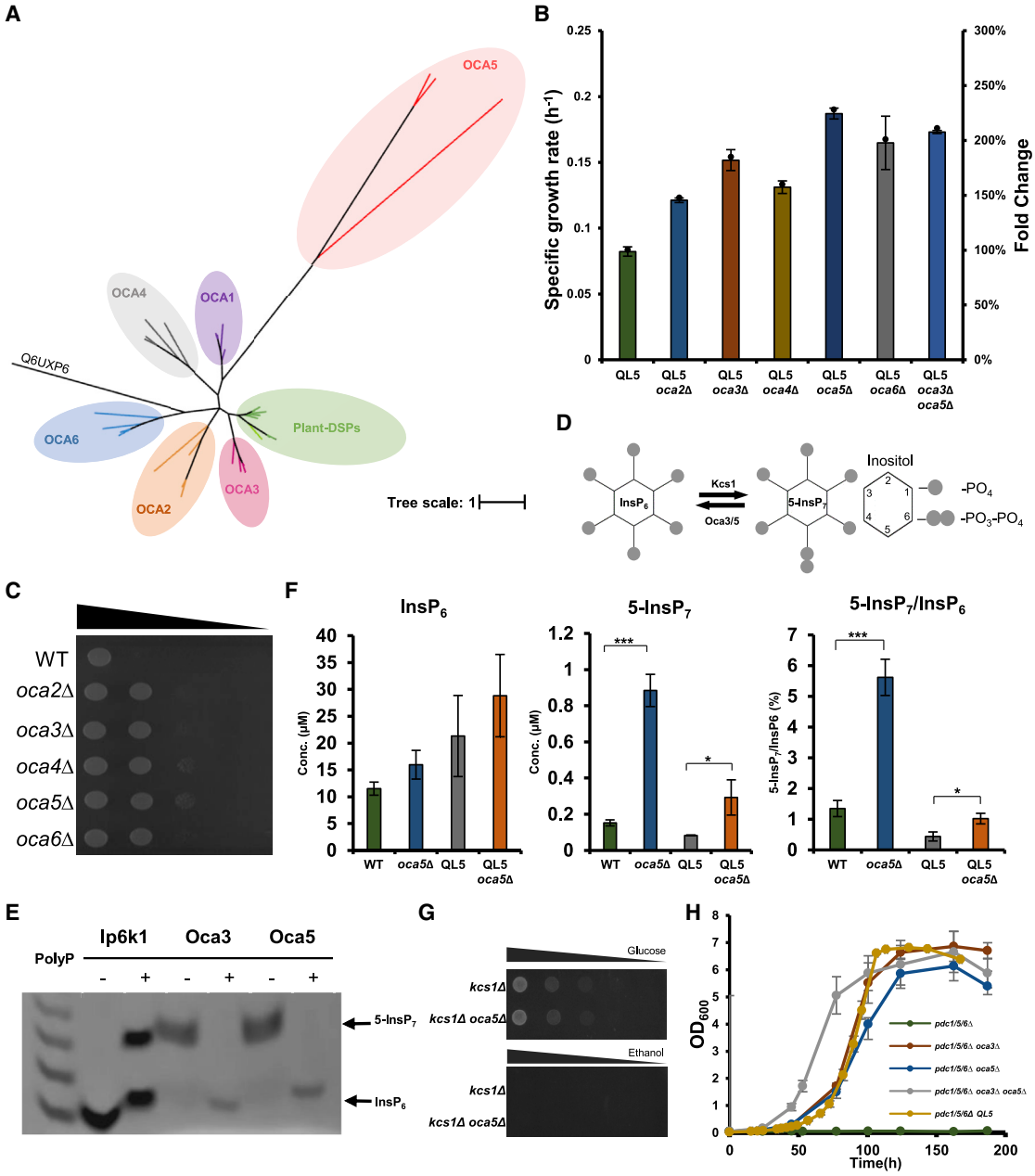

Figure 5. Oca5 was identified as an inositol pyrophosphatase in *S. cerevisiae*

(A) Phylogenetic analysis of Oca5 and OCA family proteins.

(B) μ_{max} of QL5 with deletion of different Oca family genes.

(C) Growth assay of the WT and OCA deletion strains. The strains were incubated in the minimal medium with 20 g/L ethanol and spotted by serial dilution in a plate when the OD_{600} was approximately 1.

(D) $InsP_6$ can be catalyzed by Ip6k1 to generate 5-$InsP_7$; and 5-$InsP_7$ can be degraded by Oca3 or Oca5 into $InsP_6$.

(E) Oca5 dephosphorylated 5-$InsP_7$ *in vitro*. Ip6k1 phosphorylated $InsP_6$ into 5-$InsP_7$ while both Oca3 and Oca5 dephosphorylated 5-$InsP_7$ into $InsP_6$, which were then separated using polyacrylamide-gel (PAGE) gel. The reaction mixtures containing GST-Ip6k1 (+) or water (−) incubated with $InsP_6$; GST-Oca3 (+) or water (−); and GST-Oca5 (+) or water (−) were incubated with 5-$InsP_7$. The marker was inorganic polyphosphate (PolyP).

(F) *In vivo* concentration of $InsP_6$ (left), 5-$InsP_7$ (middle), and the ratio of 5-$InsP_7$ to $InsP_6$ (right) in the WT, *oca5*Δ, QL5, and QL5 *oca5*Δ strains.

(G) Spotting assay of the *kcs1*Δ and the *kcs1*Δ *oca5*Δ strain. The serial dilution was spotted in a plate with a glucose or ethanol medium when the OD_{600} was approximately 1.

(H) Growth curve of the Pdc^- strain with the individual, double deletion of *OCA3* and *OCA5*, as well as hybrid-glycolysis yeast QL5. The growth test was performed in a shake flask with a minimal medium consisting of 20 g/L glucose. The mean ± SD was based on biological triplicates.

Statistical analysis was performed using two-tailed Student's t test (*$p < 0.05$, **$p < 0.01$, ***$p < 0.001$).

See also Figures S6 and S7 and Tables S5 and S7.

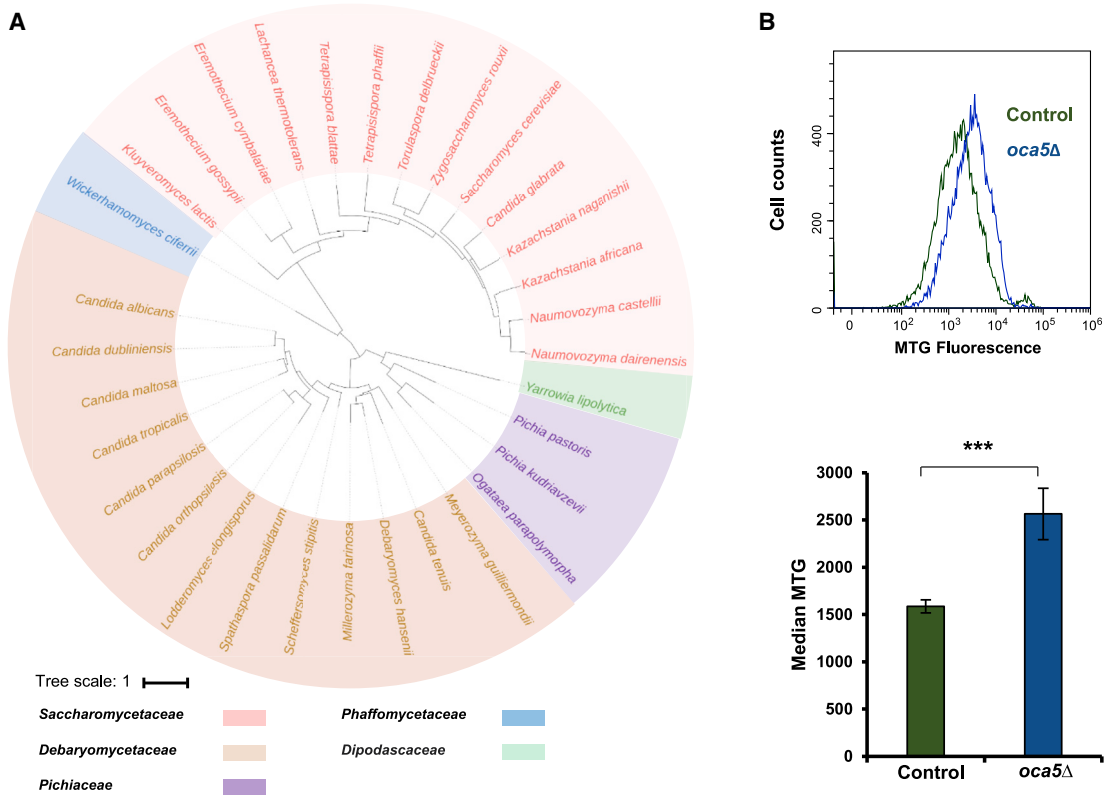

Figure 6. The phylogenetic analysis and demonstration of Oca5 in *P. pastoris*

(A) The phylogenetic tree of Oca5.

(B) Flow cytometry analyses of *P. pastoris* X-33 and *oca5*Δ after staining with MitoTracker Green (MTG) during growth on yeast extract-peptone-dextrose (YPD) medium. Samples were used during the log phase when the OD_{600} was approximately 1 in biological triplicates. The medians of MTG in flow cytometry analysis labeling of *P. pastoris* X-33 (green bars) and *P. pastoris* X-33 *oca5*Δ (blue bars). The mean ± SD were biological quintuplicates.

Statistical analysis was performed using two-tailed Student's t test (*p < 0.05, **p < 0.01, ***p < 0.001).

See also Table S7.

from 5-InsP$_7$ to InsP$_6$ on a PAGE gel, indicating that Oca5 could dephosphorylate 5-InsP$_7$ to InsP$_6$ *in vitro*, similarly to Oca3 (Figure 5E). We have also measured the concentrations of InsP$_6$ and 5-InsP$_7$ *in vivo*. After deleting *OCA5*, the concentration of 5-InsP$_7$ increased significantly both in the WT *oca5*Δ and the QL5 *oca5*Δ strain (Figure 5F). The ratio of 5-InsP$_7$ to InsP$_6$ in the WT *oca5*Δ was around 4.2-fold higher than in the WT strain and that in the QL5 *oca5*Δ it was around 2.3-fold higher than in the QL5 strain. Taken together, this supports that Oca5 is an inositol pyrophosphatase and the deletion of *OCA5* could increase the ratio of 5-InsP$_7$ to InsP$_6$ *in vivo*. Thus, Oca5 was identified as an inositol pyrophosphatase in *S. cerevisiae*.

5-InsP$_7$ is a signaling molecule that carries energy-rich diphosphate bonds,[14] and is the energy sensor that senses cellular ATP levels[15] to adjust the balance between glycolysis and respiration.[39] Deletion of *KCS1* resulted in a decrease of 5-InsP$_7$ concentration in yeast, thereby causing activation of glycolysis and repression of respiration.[16] The *kcs1*Δ could not grow in the ethanol medium.[16] Similarly, the *kcs1*Δ *oca5*Δ double deletion strain cannot grow in the ethanol medium (Figure 5G) indicating that the *kcs1*Δ abrogated the effects of *oca5*Δ (Figure 3E). To evaluate the hypothesis that Oca5 functions as Oca3 (an inositol pyrophosphatase) and is capable of regulating glycolysis and respiration, *OCA5* and *OCA3* were deleted in a Pdc$^-$ yeast strain (with all three pyruvate decarboxylase genes deleted). In such a strain, pyruvate generated by glycolysis cannot be degraded in the cytoplasm, and mitochondrial function is repressed by glucose (meaning that the Pdc$^-$ strain cannot grow on glucose[17]). The growth assays (Figure 5H) showed that the deletion of either *OCA5* or *OCA3* recovered growth of the Pdc$^-$ strain, which indicated that Oca5 and Oca3 both could release glucose repression of respiration. Furthermore, in the Pdc$^-$ yeast strain, the double deletion of *OCA5* or *OCA3* could increase the growth further (Figure 5H) but not in QL5 (Figure 5B). Meanwhile, we constructed the QL5 Pdc$^-$ strain. This strain could still grow on the glucose medium (Figure 5H). This result further supported that the growth of QL5 did not rely on ethanol fermentation.

To check whether Oca5 orthologs in other lineages have the same functions, we constructed the phylogenetic tree of Oca5 (Figure 6A) and selected Oca5 from the methylotrophic and

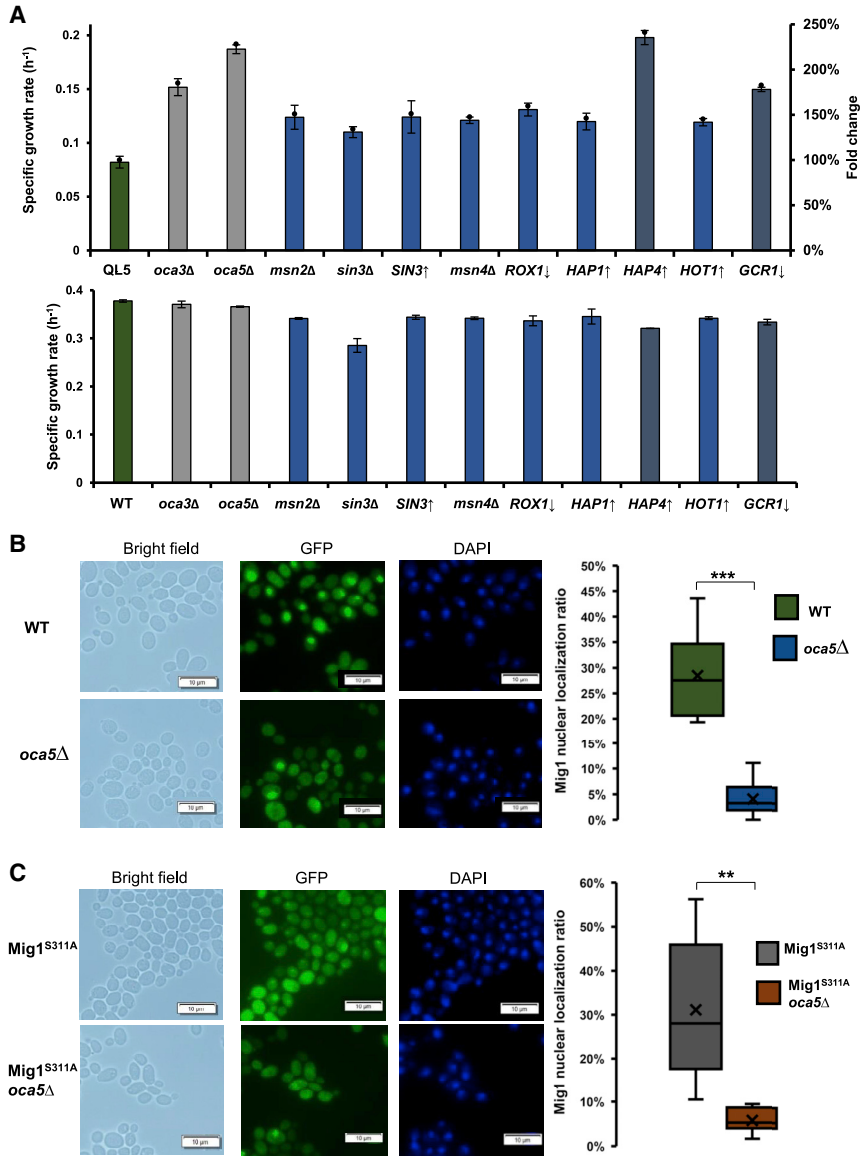

Figure 7. 5-InsP$_7$ phosphatase Oca5 affected the localization of Mig1 to cause Hap4 overexpression and recover the growth of QL5

(A) μ_{max} test of QL5 (top) and WT (bottom) with candidate TFs which were upregulated (up arrow) or downregulated (down arrow) using promoters with different activities. The used promoters for each TF were listed in Table S3. All the TFs were identified via the TF enrichment analysis results shown in Figure S4.

(B) Re-localization of Mig1 to the cytoplasm through the deletion of *OCA5*. The *MIG1* deletion strains with or without *OCA5* deletion were transformed with plasmids pUGG-Mig1-GFP.

(C) For analysis of the localization of Mig1^{S311A}, strains transformed with pUGG-Mig1^{S311A}-GFP were used for fluorescence microscopy imaging. The nuclear localization of Mig1-GFP was determined via the acquisition of octuplicate, independent images.

Statistical analysis was performed using a two-tailed Student's t test (*p < 0.05, **p < 0.01, ***p < 0.001).

See also Figure S4.

canonical Crabtree-negative yeast *Pichia pastoris.* The deletion of *OCA5* in *P. pastoris* X-33 (a different yeast strain) also increased the mitochondrial mass (Figure 6B). This result indicated that the function of Oca5 and 5-InsP$_7$ as an inositol pyrophosphatase and respiration activator, respectively, are not restricted to the Crabtree-positive yeast *S. cerevisiae*.

Mechanism underlying Oca5 regulation of glycolysis and respiration

The RNA-seq (Figure S4) and FBA (Figures 3A and 3B) results showed that Oca5 regulated cellular energy production via glycolysis and respiration. To understand the mechanism of expression regulation of genes associated with these processes in *oca5Δ*, we performed a TF enrichment analysis. Our results showed that Gcr1, which can be pyrophosphorylated by 5-InsP$_7$[16], was among the top five value significantly changed TFs in the down class (Figure S4E). Together with the top five value significantly changed TFs in the up class (Figure S4F), and TFs that in the up class significantly changed with significant regulated expressions themselves (Figure S4G), we selected TFs involved in the respiration and the metabolism of 5-InsP$_7$ for the further analyses, including Msn2, Sin3, Hot1, Rox1, Hap1, Hap4, and Gcr1. Msn4, which is regulated closely with the selected Msn2,[40] was also evaluated. Our results showed that the downregulation of *GCR1* and the upregulation of *HAP4* (Figure 7A) significantly increased QL5 cell growth. Consistently, the specific growth rate of a strain with overexpression of *HAP4* increased to 0.197 h^{-1} (even higher than *oca5Δ* and the evolved QL5-1 strains), and that of a strain with downregulation of *GCR1* increased to 0.150 h^{-1}. These results confirmed that the decreased expression of genes involved in glycolysis in *oca5Δ* (Figure 3A) was probably due to reduced activation by Gcr1.[16] Additionally, our results indicated that the increased expression of mitochondrial genes (resulting in enhanced respiration) (Figure 3B) might be mediated by the increased Hap4 activity. It is possible that such gene expression regulation was the primary cause of the dynamic regulation observed between glycolysis and respiration, subsequently resulting in the growth recovery of *oca5Δ* in QL5.

In this study, Oca5 is identified as an inositol pyrophosphatase. The link between Oca5 and Gcr1 is supported by findings showing that Gcr1 can be pyrophosphorylated by 5-InsP$_7$, resulting in an inactivation of its TF role.[16] Thus, *OCA5* deletion

increased the concentration of 5-InsP$_7$, and the subsequent Gcr1 pyrophosphorylation prevented Gcr1 from assembling into a transcription complex that would inactivate the expression of glycolytic genes. Overall, this resulted in a reduction of carbon flux through glycolysis. A mutation of Gcr1$^{(S515–8A)}$ could prevent the pyrophosphorylation of Gcrl by 5-InsP$_7$. A growth test (Table S5) showed that compared with WT, a Gcr1$^{(S515–8A)}$ strain had a lower μ_{max} and higher specific production of ethanol and glycerol, indicative of an excessive glycolytic flux. The deletion of *OCA5* recovered the cell growth and decreased ethanol and glycerol production to levels of the WT strain (Table S5). These results further confirmed that *OCA5* deletion results in a downregulated expression of glycolytic genes, owing to the 5-InsP$_7$ based pyrophosphorylation of Gcr1.

The mechanism underlying the upregulation of *HAP4* expression by 5-InsP$_7$, resulting in increased mitochondrial function, remains unclear. In yeast, Hap4 functions as the active domain of the HAP complex for the transcriptional regulation of genes involved in respiration.[41] The expression of *HAP4* is downregulated by glucose and controlled by the subcellular localization of Mig1,[42] a glucose repressor. Therefore, we characterized the subcellular localization of Mig1 (Figure 7B) and found that the deletion of *OCA5* resulted in an increased cytoplasmic presence of Mig1 under high-glucose conditions, which caused the downregulation of *HAP4* expression.

The subcellular localization of Mig1 has been reported to be determined via phosphorylation by Snf1.[43] Snf1 is the yeast AMP-activated kinase (AMPK), and the Snf1/Mig1/Hap4 glucose repression signaling pathway has been intensively studied.[44] High glucose concentrations inactivate Snf1, which when combined with the Glc7-Reg1 phosphatase, does not phosphorylate the transcription factor Mig1. In this form, the TF Mig1 is predominantly located in the nucleus,[43] where it can repress the expression of *HAP4*.[42] On the other hand, active Snf1 phosphorylates the serine 311 site of Mig1, causing it to translocate from the nucleus to the cytoplasm. This translocation results in the inhibition of Hap4 repression.[45] To evaluate if the translocation of Mig1 regulated by 5-InsP$_7$ was through Snf1, we introduced the Mig1^{S311A} mutation that would inhibit phosphorylation of Mig1 by Snf1. We found that despite the Mig1 mutation, *OCA5* deletion resulted in the translocation of Mig1 to the cytoplasm (Figure 7C). This result showed that the translocation of Mig1 to the cytoplasm under *OCA5* deletion was independent of Snf1, which clearly shows that *OCA5* directly regulates *HAP4* expression and therefore largely determines the rates of respiratory activities.

Mutations in Oca3 have been reported in multiple Crabtree-negative yeast adaptive evolutions studies (Figure S7).[17,23] These studies indicated that the convergent mutations in inositol pyrophosphatases (in our case Oca5) occurred to compensate for central carbon metabolism remodeling.[17,23] Inositol pyrophosphate include versatile messenger molecules that mediate a variety of cellular functions,[46] with 5-InsP$_7$ being regarded as the energy sensor.[47] In *S. cerevisiae*, it has been demonstrated that 5-InsP$_7$ regulated glycolysis through Gcr1.[16] Our study reports that 5-InsP$_7$ also upregulates respiration, through the translocation of Mig1 to the cytoplasm, which upregulates the expression of *HAP4*. Such regulation of mitochondrial respiration by 5-InsP$_7$ was also observed in the Crabtree-negative yeast *P. pastoris* (Figure 6), as well as in mammalian cells. For instance, the deletion of *IP6K2*, the homolog of *KCS1*, decreased the gene expression of cytochrome *c*1 and repressed the activity of complex III in brain cells.[47] Elevated 5-InsP$_7$ levels resulted in increased ATP levels, by 35%, in cancer cell lines.[48] However, current 5-InsP$_7$ studies are based on IP6Ks, and no inositol pyrophosphatase has yet been identified in higher eukaryotes. In this study, we demonstrated that although Oca5 is phylogenetically distant from other members of the Oca family, Oca5 is identified as an inositol pyrophosphatase that ensures the balancing of flux between glycolysis and respiration.

In summary, the results of the present study demonstrate the causality and impacts of hybrid-glycolysis yeast on basic and applied research. Compiling studies related to 5-InsP$_7$ were restricted to Ip6ks, which catalyze the generation of 5-InsP$_7$ in mammalian cells. We identified Oca5 as an inositol pyrophosphatase that could regulate glycolysis through Gcrl, and respiration through the Mig1/Hap4 signaling pathway independent of the Snf1. This finding was a crucial complement to the mechanism of inositol pyrophosphate as an energy sensor for balancing the flux of glycolysis and respiration. Our study highlights the importance of inositol pyrophosphate as a signal molecule in cellular metabolism and provides insights on how yeast can survive under energy shortage pressure through metabolism plasticity via the regulation of several different TFs.

Limitations of the study

The scope of this study did not include a comprehensive study of the Oca5 and 5-InsP$_7$ of a wide range of eukaryotic species, but instead focused on their impacts on the model organism *S. cerevisiae* (having the Crabtree effect) with an extended vision of the methylotrophic yeast *P. pastoris* (without the Crabtree effect). Our study shows that InsPs mechanisms are crucial to the cell's energy metabolism and need to be strictly regulated. However, research related to inositol pyrophosphatase is currently limited. Future efforts could be paid to study the response to the disturbance of this candidate inositol pyrophosphatase in higher eukaryotic organisms such as mammalian cells. Additionally, the promising activities of other Oca proteins besides Oca3 and Oca5 could also be dissected, especially on their effects on central carbon metabolism.

STAR★METHODS

Detailed methods are provided in the online version of this paper and include the following:

- KEY RESOURCES TABLE
- RESOURCE AVAILABILITY
  - Lead contact
  - Materials availability
  - Data and code availability
- EXPERIMENTAL MODEL AND SUBJECT DETAILS
  - Strains and medium
- METHOD DETAILS
  - Genetic manipulation
  - Growth analyses and shake flask fermentation

- Adaptive laboratory evolution
- Bioreactor culture
- Analytical methods
- Determination of cofactor and ATP/ADP ratio
- Systems biology analysis
- Phylogenetic analysis
- Structure alignment of Oca5 and Oca3 in yeast
- Purification of recombinant proteins
- Generation and isolation of 5-diphosphoinositol pentakisphosphate (5-InsP$_7$)
- Identification and quantification of 5-InsP$_7$ using LC-MS
- Purification of inositol phosphates by titanium dioxide pull-down
- *In vivo* analysis of InsPs by CE-ESI-MS
- Oca5 activity assay
- Flow cytometric analysis for MitoTracker green staining of mitochondria
- Isotope labeling
- Microscopy imaging

● QUANTIFICATION AND STATISTICAL ANALYSIS

SUPPLEMENTAL INFORMATION

Supplemental information can be found online at https://doi.org/10.1016/j.cell.2023.01.014.

ACKNOWLEDGMENTS

This work was supported by National Key Research and Development Program of China (2018YFA0900100), National Natural Science Foundation of China (21908004) and (22011530113), Fundamental Research Funds for the Central Universities (buctrc201801), the Beijing Advanced Innovation Center for Soft Matter Science and Engineering, Beijing University of Chemical Technology, the Novo Nordisk Foundation (NNF10CC1016517), the Knut and Alice Wallenberg Foundation, and the <u>Deutsche Forschungsgemeinschaft (DFG) under Germany's Excellence Strategy (CIBSS, EXC-2189, Project ID 390939984). We appreciate Guizhen Liu from University of Freiburg, Albertstr. for helping us prepare the InsPs samples; Verena Siewers from Chalmers University of Technology for advice on manuscript revision.

AUTHOR CONTRIBUTIONS

N.Q., Z.L., and J.N. designed the research; N.Q., L.L., X.J., R.P., Yu Chen, S.Y., Chaokun Li, X.W., H.L., G.D., D.Q., and J.J. carried out the experiment; N.Q., Yueping Zhang, Yiming Zhang, S.S., Christer Larsson, Yun Chen, T.T., Z.L, J.X., H.J.J, and J.N. analyzed the data; N.Q., Z.L., and J.N. wrote the paper. Z.L. and J.N. supervised the research.

DECLARATION OF INTERESTS

The authors declare no competing interests.

Received: May 26, 2022
Revised: July 29, 2022
Accepted: January 11, 2023
Published: February 8, 2023

REFERENCES

1. Flamholz, A., Noor, E., Bar-Even, A., Liebermeister, W., and Milo, R. (2013). Glycolytic strategy as a tradeoff between energy yield and protein cost. Proc. Natl. Acad. Sci. USA. *110*, 10039–10044. https://doi.org/10.1073/pnas.1215283110.
2. Embden, G., Deuticke, H.J., and Kraft, G. (1933). Über die Intermediären Vorgänge bei der Glykolyse in der Muskulatur. Klin. Wochenschr. *12*, 213–215. https://doi.org/10.1007/BF01757728.
3. Entner, N., and Doudoroff, M. (1952). Glucose and gluconic acid oxidation of *Pseudomonas saccharophila*. J. Biol. Chem. *196*, 853–862.
4. Burma, D.P., and Horecker, B.L. (1958). Pentose fermentation by *Lactobacillus plantarum*. J. Biol. Chem. *231*, 1039–1051.
5. de Vries, W., Gerbrandy, S.J., and Stouthamer, A.H. (1967). Carbohydrate metabolism in *Bifidobacterium bifidum*. Biochim. Biophys. Acta *136*, 415–425. https://doi.org/10.1016/0304-4165(67)90001-3.
6. Romano, A.H., and Conway, T. (1996). Evolution of carbohydrate metabolic pathways. Res. Microbiol. *147*, 448–455. https://doi.org/10.1016/0923-2508(96)83998-2.
7. Bogorad, I.W., Lin, T.S., and Liao, J.C. (2013). Synthetic non-oxidative glycolysis enables complete carbon conservation. Nature *502*, 693–697. https://doi.org/10.1038/nature12575.
8. Krusemann, J.L., Lindner, S.N., Dempfle, M., Widmer, J., Arrivault, S., Debacker, M., He, H., Kubis, A., Chayot, R., Anissimova, M., et al. (2018). Artificial pathway emergence in central metabolism from three recursive phosphoketolase reactions. FEBS J. *285*, 4367–4377. https://doi.org/10.1111/febs.14682.
9. Lin, P.P., Jaeger, A.J., Wu, T.Y., Xu, S.C., Lee, A.S., Gao, F., Chen, P.W., and Liao, J.C. (2018). Construction and evolution of an *Escherichia coli* strain relying on nonoxidative glycolysis for sugar catabolism. Proc. Natl. Acad. Sci. USA. *115*, 3538–3546. https://doi.org/10.1073/pnas.1802191115.
10. Nielsen, J., and Keasling, J.D. (2016). Engineering cellular metabolism. Cell *164*, 1185–1197. https://doi.org/10.1016/j.cell.2016.02.004.
11. Lin, S.C., and Hardie, D.G. (2018). AMPK: sensing glucose as well as cellular energy status. Cell Metab. *27*, 299–313. https://doi.org/10.1016/j.cmet.2017.10.009.
12. Usaite, R., Jewett, M.C., Oliveira, A.P., Yates, J.R., Olsson, L., and Nielsen, J. (2009). Reconstruction of the yeast Snf1 kinase regulatory network reveals its role as a global energy regulator. Mol. Syst. Biol. *5*, 319. https://doi.org/10.1038/msb.2009.67.
13. Dennis, P.B., Jaeschke, A., Saitoh, M., Fowler, B., Kozma, S.C., and Thomas, G. (2001). Mammalian TOR: a homeostatic ATP sensor. Science *294*, 1102–1105. https://doi.org/10.1126/science.1063518.
14. Shah, A., Ganguli, S., Sen, J., and Bhandari, R. (2017). Inositol pyrophosphates: energetic, omnipresent and versatile signalling molecules. J. Indian Inst. Sci. *97*, 23–40. https://doi.org/10.1007/s41745-016-0011-3.
15. Wundenberg, T., and Mayr, G.W. (2012). Synthesis and biological actions of diphosphoinositol phosphates (inositol pyrophosphates), regulators of cell homeostasis. Biol. Chem. *393*, 979–998. https://doi.org/10.1515/hsz-2012-0133.
16. Szijgyarto, Z., Garedew, A., Azevedo, C., and Saiardi, A. (2011). Influence of inositol pyrophosphates on cellular energy dynamics. Science *334*, 802–805. https://doi.org/10.1126/science.1211908.
17. Dai, Z., Huang, M., Chen, Y., Siewers, V., and Nielsen, J. (2018). Global rewiring of cellular metabolism renders *Saccharomyces cerevisiae* Crabtree negative. Nat. Commun. *9*, 3059. https://doi.org/10.1038/s41467-018-05409-9.
18. Webb, B.A., Forouhar, F., Szu, F.E., Seetharaman, J., Tong, L., and Barber, D.L. (2015). Structures of human phosphofructokinase-1 and atomic basis of cancer-associated mutations. Nature *523*, 111–114. https://doi.org/10.1038/nature14405.
19. Benisch, F., and Boles, E. (2014). The bacterial Entner-Doudoroff pathway does not replace glycolysis in *Saccharomyces cerevisiae* due to the lack of activity of iron-sulfur cluster enzyme 6-phosphogluconate

dehydratase. J. Biotechnol. *171*, 45–55. https://doi.org/10.1016/j.jbiotec.2013.11.025.

20. Bergman, A., Siewers, V., Nielsen, J., and Chen, Y. (2016). Functional expression and evaluation of heterologous phosphoketolases in *Saccharomyces cerevisiae*. Amb. Express *6*, 115. https://doi.org/10.1186/s13568-016-0290-0.
21. Meadows, A.L., Hawkins, K.M., Tsegaye, Y., Antipov, E., Kim, Y., Raetz, L., Dahl, R.H., Tai, A., Mahatdejkul-Meadows, T., Xu, L., et al. (2016). Rewriting yeast central carbon metabolism for industrial isoprenoid production. Nature *537*, 694–697. https://doi.org/10.1038/nature19769.
22. Kuser, P.R., Krauchenco, S., Antunes, O.A., and Polikarpov, I. (2000). The high resolution crystal structure of yeast hexokinase PII with the correct primary sequence provides new insights into its mechanism of action. J. Biol. Chem. *275*, 20814–20821. https://doi.org/10.1074/jbc.M910412199.
23. Zhang, Y., Liu, G., Engqvist, M.K.M., Krivoruchko, A., Hallström, B.M., Chen, Y., Siewers, V., and Nielsen, J. (2015). Adaptive mutations in sugar metabolism restore growth on glucose in a pyruvate decarboxylase negative yeast strain. Microb. Cell Fact. *14*, 116. https://doi.org/10.1186/s12934-015-0305-6.
24. Ma, H., Bloom, L.M., Zhu, Z.M., Walsh, C.T., and Botstein, D. (1989). Isolation and characterization of mutations in the *HXK2* gene of *Saccharomyces cerevisiae*. Mol. Cell Biol. *9*, 5630–5642. https://doi.org/10.1128/mcb.9.12.5630-5642.1989.
25. Kraakman, L.S., Winderickx, J., Thevelein, J.M., and De Winde, J.H. (1999). Structure-function analysis of yeast hexokinase: structural requirements for triggering cAMP signalling and catabolite repression. Biochem. J. *343 Pt 1*, 159–168.
26. Stockl, P., Zankl, C., Hutter, E., Unterluggauer, H., Laun, P., Heeren, G., Bogengruber, E., Herndler-Brandstetter, D., Breitenbach, M., and Jansen-Durr, P. (2007). Partial uncoupling of oxidative phosphorylation induces premature senescence in human fibroblasts and yeast mother cells. Free Radic. Biol. Med. *43*, 947–958. https://doi.org/10.1016/j.freeradbiomed.2007.06.005.
27. Nielsen, J. (2019). Yeast systems biology: model organism and cell factory. Biotechnol. J. *14*, e1800421. https://doi.org/10.1002/biot.201800421.
28. Patil, K.R., and Ralser, M. (2018). Freeing yeast from alcohol addiction (Just) to make (It) fat instead. Cell *174*, 1342–1344. https://doi.org/10.1016/j.cell.2018.08.024.
29. Yu, T., Zhou, Y.J., Huang, M., Liu, Q., Pereira, R., David, F., and Nielsen, J. (2018). Reprogramming yeast metabolism from alcoholic fermentation to lipogenesis. Cell *174*, 1549–1558.e14. https://doi.org/10.1016/j.cell.2018.07.013.
30. Zhou, Y.J., Buijs, N.A., Zhu, Z., Qin, J., Siewers, V., and Nielsen, J. (2016). Production of fatty acid-derived oleochemicals and biofuels by synthetic yeast cell factories. Nat. Commun. *7*, 11709. https://doi.org/10.1038/ncomms11709.
31. Zhu, Z., Hu, Y., Teixeira, P.G., Pereira, R., Chen, Y., Siewers, V., and Nielsen, J. (2020). Multidimensional engineering of *Saccharomyces cerevisiae* for efficient synthesis of medium-chain fatty acids. Nat. Catal. *3*, 64–74. https://doi.org/10.1038/s41929-019-0409-1.
32. Benschop, J.J., Brabers, N., van Leenen, D., Bakker, L.V., van Deutekom, H.W.M., van Berkum, N.L., Apweiler, E., Lijnzaad, P., Holstege, F.C.P., and Kemmeren, P. (2010). A consensus of core protein complex compositions for *Saccharomyces cerevisiae*. Mol. Cell *38*, 916–928. https://doi.org/10.1016/j.molcel.2010.06.002.
33. Mulleder, M., Calvani, E., Alam, M.T., Wang, R.K., Eckerstorfer, F., Zelezniak, A., and Ralser, M. (2016). Functional metabolomics describes the yeast biosynthetic regulome. Cell *167*, 553–565.e12. e512. https://doi.org/10.1016/j.cell.2016.09.007.
34. Decourty, L., Malabat, C., Frachon, E., Jacquier, A., and Saveanu, C. (2021). Investigation of RNA metabolism through large-scale genetic interaction profiling in yeast. Nucleic Acids Res. *49*, 8535–8555. https://doi.org/10.1093/nar/gkab680.
35. Steidle, E.A., Chong, L.S., Wu, M., Crooke, E., Fiedler, D., Resnick, A.C., and Rolfes, R.J. (2016). A novel inositol pyrophosphate phosphatase in *Saccharomyces cerevisiae*: Siw14 protein selectively cleaves the β-phosphate from 5-diphosphoinositol pentakisphosphate (5PP-IP5). J. Biol. Chem. *291*, 6772–6783. https://doi.org/10.1074/jbc.M116.714907.
36. Saiardi, A., Erdjument-Bromage, H., Snowman, A.M., Tempst, P., and Snyder, S.H. (1999). Synthesis of diphosphoinositol pentakisphosphate by a newly identified family of higher inositol polyphosphate kinases. Curr. Biol. *9*, 1323–1326. https://doi.org/10.1016/S0960-9822(00)80055-X.
37. Loss, O., Azevedo, C., Szijgyarto, Z., Bosch, D., and Saiardi, A. (2011). Preparation of quality inositol pyrophosphates. JoVE *55*, e3027. https://doi.org/10.3791/3027.
38. Losito, O., Szijgyarto, Z., Resnick, A.C., and Saiardi, A. (2009). Inositol pyrophosphates and their unique metabolic complexity: analysis by gel electrophoresis. PLoS One *4*, e5580. https://doi.org/10.1371/journal.pone.0005580.
39. Wu, M., Chong, L.S., Perlman, D.H., Resnick, A.C., and Fiedler, D. (2016). Inositol polyphosphates intersect with signaling and metabolic networks via two distinct mechanisms. Proc. Natl. Acad. Sci. USA. *113*, E6757–E6765. https://doi.org/10.1073/pnas.1606853113.
40. Steidle, E.A., Morrissette, V.A., Fujimaki, K., Chong, L., Resnick, A.C., Capaldi, A.P., and Rolfes, R.J. (2020). The InsP7 phosphatase Siw14 regulates inositol pyrophosphate levels to control localization of the general stress response transcription factor Msn2. J. Biol. Chem. *295*, 2043–2056. https://doi.org/10.1074/jbc.RA119.012148.
41. Mao, Y., and Chen, C. (2019). The hap complex in yeasts: structure, assembly mode, and gene regulation. Front. Microbiol. *10*, 1645. https://doi.org/10.3389/fmicb.2019.01645.
42. Lundin, M., Nehlin, J.O., and Ronne, H. (1994). Importance of a flanking AT-rich region in target site recognition by the GC box-binding zinc finger protein MIG1. Mol. Cell Biol. *14*, 1979–1985. 1985. https://doi.org/10.1128/mcb.14.3.1979-1985.1994.
43. Treitel, M.A., and Carlson, M. (1995). Repression by SSN6-TUP1 is directed by MIG1, a repressor/activator protein. Proc. Natl. Acad. Sci. USA. *92*, 3132–3136. https://doi.org/10.1073/pnas.92.8.3132.
44. Guaragnella, N., Coyne, L.P., Chen, X.J., and Giannattasio, S. (2018). Mitochondria–cytosol–nucleus crosstalk: learning from *Saccharomyces cerevisiae*. FEMS Yeast Res. *18*, foy088. https://doi.org/10.1093/femsyr/foy088.
45. Ahuatzi, D., Riera, A., Pelaez, R., Herrero, P., and Moreno, F. (2007). Hxk2 regulates the phosphorylation state of Mig1 and therefore its nucleocytoplasmic distribution. J. Biol. Chem. *282*, 4485–4493. https://doi.org/10.1074/jbc.M606854200.
46. Ganguli, S., Shah, A., Hamid, A., Singh, A., Palakurti, R., and Bhandari, R. (2020). A high energy phosphate jump-from pyrophospho-inositol to pyrophospho-serine. Adv. Biol. Regul. *75*, 100662. https://doi.org/10.1016/j.jbior.2019.100662.
47. Nagpal, L., Kornberg, M.D., Albacarys, L.K., and Snyder, S.H. (2021). Inositol hexakisphosphate kinase-2 determines cellular energy dynamics by regulating creatine kinase-B. Proc. Natl. Acad. Sci. USA. *118*, e2020695118. https://doi.org/10.1073/pnas.2020695118.
48. Gu, C., Nguyen, H.N., Ganini, D., Chen, Z., Jessen, H.J., Gu, Z., Wang, H., and Shears, S.B. (2017). KO of 5-InsP$_7$ kinase activity transforms the HCT116 colon cancer cell line into a hypermetabolic, growth-inhibited phenotype. Proc. Natl. Acad. Sci. USA. *114*, 11968–11973. https://doi.org/10.1073/pnas.1702370114.
49. Deatherage, D.E., and Barrick, J.E. (2014). Identification of mutations in laboratory-evolved microbes from next-generation sequencing data using breseq. Methods Mol. Biol. *1151*, 165–188. https://doi.org/10.1007/978-1-4939-0554-6_12.

50. Langmead, B., and Salzberg, S.L. (2012). Fast gapped-read alignment with Bowtie 2. Nat. Methods *9*, 357–359. https://doi.org/10.1038/nmeth.1923.

51. Varemo, L., Nielsen, J., and Nookaew, I. (2013). Enriching the gene set analysis of genome-wide data by incorporating directionality of gene expression and combining statistical hypotheses and methods. Nucleic Acids Res. *41*, 4378–4391. https://doi.org/10.1093/nar/gkt111.

52. Heirendt, L., Arreckx, S., Pfau, T., Mendoza, S.N., Richelle, A., Heinken, A., Haraldsdottir, H.S., Wachowiak, J., Keating, S.M., Vlasov, V., et al. (2019). Creation and analysis of biochemical constraint-based models using the COBRA Toolbox v.3.0. Nat. Protoc. *14*, 639–702. https://doi.org/10.1038/s41596-018-0098-2.

53. Jumper, J., Evans, R., Pritzel, A., Green, T., Figurnov, M., Ronneberger, O., Tunyasuvunakool, K., Bates, R., Žídek, A., Potapenko, A., et al. (2021). Highly accurate protein structure prediction with AlphaFold. Nature *596*, 583–589. https://doi.org/10.1038/s41586-021-03819-2.

54. Li, Z., Jaroszewski, L., Iyer, M., Sedova, M., and Godzik, A. (2020). FATCAT 2.0: towards a better understanding of the structural diversity of proteins. Nucleic Acids Res. *48*, W60–W64. https://doi.org/10.1093/nar/gkaa443.

55. Letunic, I., and Bork, P. (2021). Interactive Tree Of Life (iTOL) v5: an online tool for phylogenetic tree display and annotation. Nucleic Acids Res. *49*, W293–W296. https://doi.org/10.1093/nar/gkab301.

56. Kumar, S., Stecher, G., Li, M., Knyaz, C., and Tamura, K. (2018). MEGA X: molecular evolutionary genetics analysis across computing platforms. Mol. Biol. Evol. *35*, 1547–1549. https://doi.org/10.1093/molbev/msy096.

57. van Dijken, J.P., Bauer, J., Brambilla, L., Duboc, P., Francois, J.M., Gancedo, C., Giuseppin, M.L., Heijnen, J.J., Hoare, M., Lange, H.C., et al. (2000). An interlaboratory comparison of physiological and genetic properties of four *Saccharomyces cerevisiae* strains. Enzyme Microb. Technol. *26*, 706–714. https://doi.org/10.1016/s0141-0229(00)00162-9.

58. Verduyn, C., Postma, E., Scheffers, W.A., and Van Dijken, J.P. (1992). Effect of benzoic acid on metabolic fluxes in yeasts: a continuous-culture study on the regulation of respiration and alcoholic fermentation. Yeast *8*, 501–517. https://doi.org/10.1002/yea.320080703.

59. Zhang, Y., Wang, J., Wang, Z., Zhang, Y., Shi, S., Nielsen, J., and Liu, Z. (2019). A gRNA-tRNA array for CRISPR-Cas9 based rapid multiplexed genome editing in *Saccharomyces cerevisiae*. Nat. Commun. *10*, 1053. https://doi.org/10.1038/s41467-019-09005-3.

60. Zaldivar, J., Borges, A., Johansson, B., Smits, H.P., Villas- Bôas, S.G., Nielsen, J., and Olsson, L. (2002). Fermentation performance and intracellular metabolite patterns in laboratory and industrial xylose-fermenting *Saccharomyces cerevisiae*. Appl. Microbiol. Biotechnol. *59*, 436–442. https://doi.org/10.1007/s00253-002-1056-y.

61. Nissen, T.L., Anderlund, M., Nielsen, J., Villadsen, J., and Kielland-Brandt, M.C. (2001). Expression of a cytoplasmic transhydrogenase in *Saccharomyces cerevisiae* results in formation of 2-oxoglutarate due to depletion of the NADPH pool. Yeast *18*, 19–32. CO;2-5. https://doi.org/10.1002/1097-0061(200101)18:1<19::AID-YEA650>3.0.

62. Guldener, U., Heck, S., Fielder, T., Beinhauer, J., and Hegemann, J.H. (1996). A new efficient gene disruption cassette for repeated use in budding yeast. Nucleic Acids Res. *24*, 2519–2524. https://doi.org/10.1093/nar/24.13.2519.

63. Melo, N.T.M., Mulder, K.C.L., Nicola, A.M., Carvalho, L.S., Menino, G.S., Mulinari, E., and Parachin, N.S. (2018). Effect of pyruvate decarboxylase knockout on product distribution using *Pichia pastoris* (*Komagataella phaffii*) engineered for lactic acid production. Bioengineering (Basel) *5*, 17. https://doi.org/10.3390/bioengineering5010017.

64. Villadsen, J., Nielsen, J., and Lidén, G. (2011). Bioreaction Engineering Principles (Boston, MA: Springer) https://doi.org/10.1007/978-1-4419-9688-6.

65. Dunn, W.B., and Winder, C.L. (2011). Sample preparation related to the intracellular metabolome of yeast methods for quenching, extraction, and metabolite quantitation. Methods Enzymol. *500*, 277–297. https://doi.org/10.1016/B978-0-12-385118-5.00015-3.

66. Xia, J., Sanchez, B.J., Chen, Y., Campbell, K., Kasvandik, S., and Nielsen, J. (2022). Proteome allocations change linearly with the specific growth rate of *Saccharomyces cerevisiae* under glucose limitation. Nat. Commun. *13*, 2819. https://doi.org/10.1038/s41467-022-30513-2.

67. Qin, N., Li, L., Ji, X., Li, X., Zhang, Y., Larsson, C., Chen, Y., Nielsen, J., and Liu, Z. (2020). Rewiring central carbon metabolism ensures increased provision of acetyl-CoA and NADPH required for 3-OH-propionic acid production. ACS Synth. Biol. *9*, 3236–3244. https://doi.org/10.1021/acssynbio.0c00264.

68. Oliveira, A.P., Patil, K.R., and Nielsen, J. (2008). Architecture of transcriptional regulatory circuits is knitted over the topology of bio-molecular interaction networks. BMC Syst. Biol. *2*, 17. https://doi.org/10.1186/1752-0509-2-17.

69. Lu, H., Li, F., Sánchez, B.J., Zhu, Z., Li, G., Domenzain, I., Marcišauskas, S., Anton, P.M., Lappa, D., Lieven, C., et al. (2019). A consensus *S. cerevisiae* metabolic model Yeast8 and its ecosystem for comprehensively probing cellular metabolism. Nat. Commun. *10*, 3586. https://doi.org/10.1038/s41467-019-11581-3.

70. Lewis, N.E., Hixson, K.K., Conrad, T.M., Lerman, J.A., Charusanti, P., Polpitiya, A.D., Adkins, J.N., Schramm, G., Purvine, S.O., Lopez-Ferrer, D., et al. (2010). Omic data from evolved *E. coli* are consistent with computed optimal growth from genome-scale models. Mol. Syst. Biol. *6*, 390. https://doi.org/10.1038/msb.2010.47.

71. Mahadevan, R., and Schilling, C.H. (2003). The effects of alternate optimal solutions in constraint-based genome-scale metabolic models. Metab. Eng. *5*, 264–276. https://doi.org/10.1016/j.ymben.2003.09.002.

72. Haraldsdottir, H.S., Cousins, B., Thiele, I., Fleming, R.M.T., and Vempala, S. (2017). CHRR: coordinate hit-and-run with rounding for uniform sampling of constraint-based models. Bioinformatics *33*, 1741–1743. https://doi.org/10.1093/bioinformatics/btx052.

73. Lemoine, F., Correia, D., Lefort, V., Doppelt-Azeroual, O., Mareuil, F., Cohen-Boulakia, S., and Gascuel, O. (2019). NGPhylogeny.fr: new generation phylogenetic services for non-specialists. Nucleic Acids Res. *47*, W260–W265. https://doi.org/10.1093/nar/gkz303.

74. Qiu, D., Wilson, M.S., Eisenbeis, V.B., Harmel, R.K., Riemer, E., Haas, T.M., Wittwer, C., Jork, N., Gu, C., Shears, S.B., et al. (2020). Analysis of inositol phosphate metabolism by capillary electrophoresis electrospray ionization mass spectrometry. Nat. Commun. *11*, 6035. https://doi.org/10.1038/s41467-020-19928-x.

75. Wilson, M.S., and Saiardi, A. (2018). Inositol phosphates purification using titanium dioxide beads. Bio. Protoc. *8*, e2959. https://doi.org/10.21769/BioProtoc.2959.

76. Qiu, D., Eisenbeis, V.B., Saiardi, A., and Jessen, H.J. (2021). Absolute quantitation of inositol pyrophosphates by capillary electrophoresis electrospray ionization mass spectrometry. JoVE *2021*, 1–13. https://doi.org/10.3791/62847.

77. Harmel, R.K., Puschmann, R., Nguyen Trung, M., Saiardi, A., Schmieder, P., and Fiedler, D. (2019). Harnessing ^{13}C-labeled myo-inositol to interrogate inositol phosphate messengers by NMR. Chem. Sci. *10*, 5267–5274. https://doi.org/10.1039/c9sc00151d.

78. Farre, J.C., Shirahama-Noda, K., Zhang, L., Booher, K., and Subramani, S. (2007). Localization of proteins and organelles using fluorescence microscopy. Methods Mol. Biol. *389*, 239–250. https://doi.org/10.1007/978-1-59745-456-8_17.

79. Canelas, A.B., ten Pierick, A., Ras, C., Seifar, R.M., van Dam, J.C., van Gulik, W.M., and Heijnen, J.J. (2009). Quantitative evaluation of intracellular metabolite extraction techniques for yeast metabolomics. Anal. Chem. *81*, 7379–7389. https://doi.org/10.1021/ac900999t.

80. Benjamini, Y., and Hochberg, Y. (1995). Controlling the False Discovery Rate: A Practical and Powerful Approach to Multiple Testing. J. Roy.

Stat. Soc. B *57*, 289–300. https://doi.org/10.1111/j.2517-6161.1995.tb02031.x.

81. Keren, L., Zackay, O., Lotan-Pompan, M., Barenholz, U., Dekel, E., Sasson, V., Aidelberg, G., Bren, A., Zeevi, D., Weinberger, A., et al. (2013). Promoters maintain their relative activity levels under different growth conditions. Mol. Syst. Biol. *9*, 701. https://doi.org/10.1038/msb.2013.59.

82. Shi, S., Chen, Y., Siewers, V., and Nielsen, J. (2014). Improving production of malonyl coenzyme A-derived metabolites by abolishing Snf1-dependent regulation of Acc1. mBio *5*. e01130–e01114. https://doi.org/10.1128/mBio.01130-14.

83. Florio, T.J., Lokareddy, R.K., Gillilan, R.E., and Cingolani, G. (2019). Molecular Architecture of the Inositol Phosphatase Siw14. Biochemistry *58*, 534–545. https://doi.org/10.1021/acs.biochem.8b01044.

STAR★METHODS

KEY RESOURCES TABLE

REAGENT or RESOURCE	SOURCE	IDENTIFIER
Chemicals, peptides, and recombinant proteins		
Phytic acid solution	Sigma-Aldrich	593648
ATP (Mg salt)	Sigma-Aldrich	A9187
Creatine phosphokinase	Sigma-Aldrich	C3755
C8 - C22, certified reference material	Sigma-Aldrich	CRM18920
Boron trifluoride-methanol	Sigma-Aldrich	B1252
Pentadecanoic acid	Fisher	A14664-30
MitoTracker™ Green FM	Fisher	M7514
D-Glucose-1-^{13} C	Sigma-Aldrich	297046
carbonyl cyanide 3-chlorophenylhydrazone	Sigma-Aldrich	C2759
NADP/NADPH Quantitation Kit	Sigma-Aldrich	MAK038
NAD/NADH Quantitation Kit	Sigma-Aldrich	MAK037
ATP Determination Kit	Fisher	A22066
Pierce™ Protein Concentrators PES, 10K MWCO, 0.5 mL	Sigma-Aldrich	88513
Pyruvate Kinase from rabbit muscle	Sigma-Aldrich	P9136
Cytidine 5′-triphosphate disodium salt	Sigma-Aldrich	C1506
Deposited data		
Genome sequence data	NCBI	PRJNA838063
RNA sequence data	NCBI	PRJNA838077
Experimental models: Organisms/strains		
S. cerevisiae CEN.PK 113-11C	Jens Lab	N/A
Pichia pastoris X-33	Jens Lab	N/A
Oligonucleotides		
For all primers, see Table S3	This paper	N/A
Recombinant DNA		
For all plasmid, see Table S2	This paper	N/A
Software and algorithms		
Breseq v0.30.2	Deatherage and Barrick[49]	https://github.com/barricklab/breseq/releases
Bowtie v2.2.8	Langmead and Salzberg[50]	https://bowtie-bio.sourceforge.net/bowtie2/index.shtml
R package (PIANO) (v.2.0.2)	Varemo et al.[51]	https://varemo.github.io/piano/
COBRA	Heirendt et al.[52]	https://github.com/opencobra/cobrapy
AlphaFold Monomer v2.0	Jumper et al.[53]	https://alphafold.ebi.ac.uk/
FATCAT 2.0	Li et al.[54]	https://fatcat.godziklab.org/
iTOL v6	Letunic and Bork[55]	https://itol.embl.de/
MEGA X	Kumar et al.[56]	https://www.megasoftware.net/

RESOURCE AVAILABILITY

Lead contact

Further information and requests could be directed to the lead contact, Zihe Liu (zihe@mail.buct.edu.cn).

Materials availability

This study did not generate new unique reagents. Details of strains and plasmids used in this study are available in Table S3. Sequences of genes, promoters, terminators, and primers are available in Table S3. Genome sequencing results of open reading fragment mutation are available in Table S4. The accession number of Oca5 homologs is available in Table S7.

Data and code availability

The accession number for the genome sequence data of evolved strains reported in this paper is [NCBI]: [PRJNA838063], https://www.ncbi.nlm.nih.gov/sra/PRJNA838063; and the accession number for the RNA sequence data of *oca5* strains reported in this paper is [NCBI]: [PRJNA838077], https://www.ncbi.nlm.nih.gov/sra/PRJNA838077. The data is publicly available as of the date of publication. This study did not generate any code or additional information.

EXPERIMENTAL MODEL AND SUBJECT DETAILS

Strains and medium

An *S. cerevisiae* strain CEN.PK 113-11C (*MATa SUC2 MAL2-8^c his3Δ1 ura3-52*)[57] was used as the experimental model in this study. All the derivatives strains and their genotype used in this study are listed in Table S3. The defined minimal medium[58] consisted of 7.5 g/L $(NH_4)_2SO_4$, 14.4 g/L KH_2PO_4, and 0.5 g/L $MgSO_4 \cdot 7H_2O$ (the pH of the medium was adjusted to 6.5 with KOH). Trace metal and vitamin solutions were supplemented after the medium was autoclaved at 121°C for 20 min. Histidine (40 mg/L) and uracil (40 mg/L) were supplemented when necessary. For the production of FFAs, the concentration of histidine and uracil were changed to 80 mg/L. For the urea fermentation of FFAs production, the 7.5 g/L $(NH_4)_2SO_4$ was changed to 2.27 g/L urea and 6.6 g/L K_2SO_4 as reported.[31] The synthetic complete dropout uracil (SC-ura) medium (Sinopharm, Beijing, China) consisted of 6.7 g/L yeast-nitrogen base (YNB) with ammonium sulfate (5 g/L), and a 0.77 g/L mix of amino acids exclude uracil. The YPD medium consisted of 10 g/L yeast extract (Oxoid, Waltham, USA) and 20 g/L peptone (Oxoid, Waltham, USA). The carbon source in all the media was 20 g/L glucose. The SC with 0.8 g/L 5-fluoroorotic acid medium was used to select against and removed the plasmid with the *URA3* maker. Details of all engineered strains could be found in Table S3.

METHOD DETAILS

Genetic manipulation

The GTR-CRISPR system[59] was used for genome modifications in *S. cerevisiae*. All plasmids were constructed by Golden Gate assembly. The genome integrated sites used were previously reported.[60] The sequence of the gene encoding transhydrogenase (*TH*; EC 1.6.1.1) was obtained from *Azotobacter vinelandii*[61]; the sequence of phosphoketolase with substrate specificity to xylulose-5-phosphate (*xPK*; EC 4.1.2.9) was from *L. mesenteroides*[20]; and the sequence of phosphotransacetylase (*PTA*; EC 2.3.1.8) was from *C. kluyveri*.[21] All three genes were codon-optimized to *S. cerevisiae* and synthesized by Sangon Biotech (Shanghai, China). The genes encoding 6-phospho-D-gluconate dehydratase (*edd*; EC 4.2.1.12) and 2-dehydro-3-deoxyd-gluconate-6-phosphate aldolase (*eda*; EC 4.1.2.14) were amplified from the genome of *E. coli* MG 1655. The truncated thioesterase *TesA* from *E. coli* and the *FAS* (*RtFAS1* and *RtFAS2*) from *Rhodosporidium toruloides* were amplified from the genome of YJC45.[30] Details of strains, DNA fragments, and primers are summarized in Table S3, respectively. For the *OCA5* deletion in *P. pastoris*, DNA fragments corresponding to the upstream and downstream (~800 bp) flanking regions of *OCA5* were amplified from the genome of *P. pastoris* X-33, together with the amplification of the *kanMX* cassette from the *pUG6* plasmid.[62] These fragments were then assembled into one DNA fragment and transformed into *P. pastoris* competent cells according to a reported method.[63] A YPD medium with 600 mg/L G418 (Sinopharm, Beijing, China) was used for positive colony screening. All DNA fragment sequences and primers are listed in Table S3.

Growth analyses and shake flask fermentation

The medium used for growth tests in shake flasks was a defined minimal medium. At the exponential phase, the strain was inoculated into a 100 mL shake flask containing 25 mL of the defined minimal medium with a final optical density at 600 nm (OD_{600}) of 0.01. The flask was then incubated at 30°C at 200 rpm. The maximum specific growth rate (μ_{max}) was calculated by the ln (OD_{600}) range from 0.1 to 1 against time. FFAs were produced in a 100 mL shake flask with 25 mL minimal medium and 20 g/L glucose, and 80 mg/L of histidine and uracil were added to the medium. The overnight pre-culture was inoculated to the initial OD_{600} 0.25 and cultured at 200 rpm and 30°C until the fermentation was completed. For the spotting analysis, the strain was pre-cultured in the shake flask with the corresponding liquid medium until log phase and spotted on a plate after serial dilution. For the CCCP spotting analysis, after the minimal medium was autoclaved and cooled to around 50°C the CCCP was added. The plate with 10 μM CCCP was stored at −4°C before being used.

Adaptive laboratory evolution

The adaptive laboratory evolution of QL5 toward growth on glucose was performed in five independent culture lines at 30°C in 100 mL shake flasks containing 20 mL defined minimal medium. The initial OD_{600} for the adaptive laboratory evolution was 0.1, and

after 4–5 generations (OD_{600} around 2–2.5), the strains were transferred into the same volume of fresh medium to OD_{600} 0.1 for the next round of evolution. After around 400 generations, three independent colonies from each flask were selected for the growth evaluation and genome sequencing.

Bioreactor culture

The defined minimal medium was used for bioreactor culture. The strain was sequentially prepared in a 50 mL Bio-Reaction Tube (BRT-010-050) and 100 mL shake flask. The pre-culture conditions were similar to those in shake flask culture. DasGip Parallel Bioreactor Systems for Microbiology (Eppendorf) was used for bioreactor culture. In the log phase, the pre-culture strain was inoculated into 500 mL defined minimal medium to OD_{600} of 0.01. The temperature was set to 30°C, and DasGip MX4/4 module was used for the aeration control; this aeration was initially provisioned at 30 L/h (1 V/V/M). Initial agitation was set to 400 rpm and was increased to a maximum value of 800 rpm; this adjustment depended on the dissolved oxygen levels. Via controlled the stirrer speed and the gas flow rate by using the DasGip control system to maintain the dissolved oxygen levels above 30%. The DasGip GA4 gas analyzer (Eppendorf) was used to examine the composition of the outflowing gas. During the course of the culture, the solutions of 1 mol/L HCl and 2 mol/L KOH was used to adjust the pH of the minimal medium to 5.0. The addition of the acid and base was performed using DasGip MP8 multi-pump modules. The detection of μ_{max} was similar to that in shake flask culture. One drop of antifoam 204 (Sigma) was added to each bioreactor. The dry cell weight (DCW) of the samples was measured gravimetrically on membrane disk filters (PES, 0.45 μm, Pall, USA). Before measuring the increased weight, 5 mL of the broth was filtered through a 0.45 μm nitrocellulose filter and then washed once with 5 mL deionized water and dried for 48 h at 70°C. The biomass composition of $CH_{1.8}O_{0.5}N_{0.2}$ was assumed.[64]

Analytical methods

The concentration of glucose and extracellular metabolites was determined using high-performance liquid chromatography (HPLC), which was performed as previously reported.[17] The culture samples were analyzed using an HPLC system (Shimadzu, Japan) with an Aminex HPX-87H column (Bio-Rad, Hercules, USA) at 45°C using 5 mM H_2SO_4 as the mobile phase at 0.5 mL/min flow rate for 30 min.

FFAs were extracted and converted to methyl esters using a modified version of a previously described method.[31] In the modified protocol, 100 μL aliquots of the sample (cells with medium) were added in glass vials and diluted 20-folds with distilled water, if the concentration of the titer was higher than 10 mg/L. Subsequently, 250 μL NaCl (10% w/v) and 250 μL acetic acid (70 mg/L pentadecanoic acid as the internal standard) were added to the vials followed by 1 mL (v/v) of the chloroform-methanol mixture. The mixture was vortexed at 1,800 rpm for 30 min and subsequently centrifuged at 1,892 *g* for 10 min to facilitate biphasic separation. Approximately, 100 μL of the lower organic phase was transferred to a vial with 500 μL boron trifluoride-methanol (14%, Sigma-Aldrich) and incubated at 25°C overnight for fatty acid methyl ester (FAME) catalysis. For the FAME extraction, 600 μL hexane and 1 mL of water were sequentially added to the vial, and the mixture was vortexed and centrifuged as previously described. From this biphasic sample, 200 μL of the upper hexane phase was used for gas chromatography (GC) analysis.

For FAME quantification, GC-MS was performed on QP 2020 (Shimadzu) with a DB-5MS column (30 m × 0.250 mm × 0.25 μm, Agilent). Sample injections of 1 μL were performed without split at 240°C. Helium was used as the carrier gas at a flow rate of 3.0 mL/min. The program was set as follows: initial temperature of the column was set to 40°C for 2 min; ramped by 5°C/min to 130°C; then 10°C/min to 280°C and held for 3 min. The temperatures of the inlet, mass transfer line, and ion source were set at 280°C, 280°C, and 230°C, respectively. The data were collected in the full scan mode over the *m/z* range of 50–650, and the quantification was conducted using GC-MS solution 4.4 software. The FAMEs were quantified by calibrated curves of each individual standard and normalized by internal standards to obtain the absolute concentration.

Determination of cofactor and ATP/ADP ratio

Cells were harvested from the batch fermentation with OD_{600} around 1. The sample preparation was performed as previously reported with slight modifications.[65,66] Briefly, 5 mL cultured media were transferred to 35 mL quenching solution (60% methanol pre-chilled to −40°C) and mixed for 1 s. The mixture was centrifuged at 5,000 *g*, −20°C for 3 min. Pellets were snap-freeze in liquid nitrogen and stored at −80°C for further experiments. The $NADP^+$/NADPH Quantitation Kit (MAK038 (Sigma-Aldrich)) and NAD^+/NADH Quantitation Kit (MAK037 (Sigma-Aldrich)) were used for the cofactor determination. Before analysis, pellets were centrifuged at 5,000 *g*, −20°C for 1 min to remove residual methanol. Pellets were then resuspended by 1 mL pre-chilled PBS buffer followed by kit instructions. 0.4 OD_{600} and 0.04 OD_{600} cells were used for the determination of NADPH ratio and NADH ratio, respectively. The cell lysis step followed the previously described method with slight modifications.[67] Cells were lysed using FastPrep-24 5G for 20 s (6.0 m/s) and the lysed cycle was repeated twice. In each interval, the sample was placed on ice for 2 min cooling. The deproteinized step in this kit was adapted as follows. Pierce Protein Concentrators PES (10K MWCO 0.5 mL, Thermo Scientific) was used to filter the supernatant which was centrifuged at 14,500 *g* for 10–15 min to remove the proteins. All steps were carried out at 0°C. The filtrate was used to measure cofactors.

ATP level was determined by ATP Determination Kit (A22066 (Thermo Fisher Scientific)) following a previously reported method with some modifications listed below.[16] Sampling preparation was similar to methods in determining cofactors. Pellets (containing

around 5 OD_{600} bacteria) were centrifuged at 5,000 *g*, −20°C for 1 min to remove residual methanol. Cells were resuspended with 250 μL ice-cold phenol/chloroform (1:1) (Sigma-Aldrich) and with 250 μL pre-chilled LETS buffer (10 mM Tris, pH 8, 100 mM LiCl, 10 mM EDTA, 0.5% SDS) and transferred to 2 mL Eppendorf tube containing around 50 μL glass beads. The mixture was vortexed for 5 min at 4°C and centrifuged at 15,000 *g* at 4°C to separate the water phase for 10 min. ATP and ADP measurements were determined by three parallels. 10 μL water phase (×3) was added to the reaction mix to determine the ATP level. Meanwhile, 30 μL water phase was added to 2× ADP reaction buffer (8.4 mM phosphoenolpyruvate, 40 mM $MgCl_2$, 16 mM KCl, 2 mM EDTA, 20 mM sucrose, 0.5 mM of cytidine triphosphate (CTP [Sigma-Aldrich C1506]), and 21 U/mL of pyruvate kinase (PK [Sigma-Aldrich P9136])) and incubated for 15 min to transform ADP to ATP. Generated ATP from ADP was measured by the same method for ATP determination. All samples should be placed at 0°C if not specified and all buffers should be pre-chilled.

Systems biology analysis

Genomic DNA sequencing was performed by GENEWIZ Co (Beijing, China). *S. cerevisiae* CEN.PK 7-D was used as the reference genome for mapping reads using the bresEq. 0.30.2 method[49] with Bowtie 2.2.8[66] as an aligner. Mutations in the yeast clones were identified using the genome sequencing data of QL5. Further, chromosome duplication and deletion were identified by analyzing the coverage map for each chromosome. The cells at OD_{600} of approximately 1 from the batch fermentation were used for transcriptome analysis and sequenced by Annoroad Co (Beijing, China). The R package (PIANO) (v.2.0.2)[67] was used for enrichment analysis. The detailed information on terms was obtained from the *Saccharomyces* Genome Database (https://www.yeastgenome.org/). Furthermore, TF analysis was performed to calculate the significance of the expression change of gene sets regulated by the TFs.[68]

The flux balance analysis (FBA) was performed to estimate the flux distributions. An *S. cerevisiae* model, Yeast8,[69] was used for FBA, according to a published study of COBRA.[52] The upper and lower limits of measured data constrained the related exchange reaction rates (Table S5). The growth rate was maximized. The estimated growth rates were confirmed by the measured growth rate values (Table S5). Flux balance analysis (FBA)[70] was performed to estimate the unique flux distribution for each strain with growth maximization as the objective function. Flux variability analysis (FVA)[71] was performed to find the minimum and maximum flux for each reaction. The sampling method[72] was performed for each strain by sampling 10,000 points.

Phylogenetic analysis

Accession numbers of amino acid sequences used for the Oca5 phylogenetic tree and Oca family phylogenetic tree generation are listed in Table S7. The sequences were aligned using MUSCLE in MEGA X[72] and trimmed using NGPhylogeny.fr.[73] MEGA X (ML using 500 bootstraps) was used to construct maximum likelihood phylogenetic tree, and iTOL v6[74] was used for the modification of the phylogenetic tree.

Structure alignment of Oca5 and Oca3 in yeast

The structure of Oca5 (P38738) in yeast was predicted using AlphaFold Monomer v2.0 pipeline.[53] Furthermore, FATCAT 2.0 (flexible mode)[54] (https://fatcat.godziklab.org/) was used to compare the structures of Oca5 and Oca3 (6byf) in yeast.

Purification of recombinant proteins

IP6K1 from *M. musculus* and *OCA3* and *OCA5* from *S. cerevisiae* were codon-optimized for protein synthesis and purification in *E. coli*. Codon-optimized genes were synthesized by Sangon Biotech (Shanghai, China). *E. coli* DH5α and pGEX-4T-1 strains were used for plasmid construction, and *E. coli* BL21 (DE3) was used for protein expression. A GST tag was added at the N-terminal of all proteins. Protein expression and purification were conducted following a previously described protocol with slight modifications.[35] Single colonies were used to inoculate 4 mL of Luria–Bertani (LB) medium with ampicillin cultivated overnight at 37°C and 200 rpm. The overnight culture was inoculated in 800 mL LB medium with ampicillin and incubated at 200 rpm and 37°C until OD_{600} of 0.6–0.8 was reached. Thereafter, isopropyl-β-*d*-thiogalactoside (IPTG; 0.1 mM final concentration) was added to the cell cultures for *IP6K1* and *OCA5* expression and incubated at 16°C for 16 h. For *OCA3* expression, IPTG was added to the corresponding cell culture at 1 mM final concentration and incubated at 13°C for 30 h. Cells were harvested by centrifugation at 1,500 *g* at 4°C for 10 min and washed with PBS (PBS). Thereafter, the cells were resuspended in PBS buffer with 3% (v/v) glycerol and stored at −80°C until further analyses.

For protein purification, glutathione Sepharose 4B (Merck) was washed with GST-lysis buffer (PBS with 2 mM fresh dithiothreitol [DTT]). Cells were disrupted using a high-pressure homogenizer crusher (JNBIO) and centrifuged at 20,000 *g* for 50 min at 4°C. Subsequently, the supernatant was incubated overnight with glutathione Sepharose buffer at 4°C and sequentially washed with the GST-lysis buffer and GST-elution buffer (50 mM Tris, 200 mM NaCl, 20 mM reduced glutathione, and 2 mM fresh DTT, pH 8.0 balanced using NaOH). The Amicon Ultra Centrifugal Filter (Millipore) was used for protein concentration and buffer exchange with dialysis buffer (100 mM NaCl, 1 mM $MgSO_4$, 1 mM DTT, 0.05% (v/v) CHAPS, and 20 mM Tris–HCl at pH 7.4). The buffers were pre-chilled to 4°C, and all steps were carried out at 4°C. Protein purification was conducted under gravitational flow.

Generation and isolation of 5-diphosphoinositol pentakisphosphate (5-InsP$_7$)

The generation and isolation of 5-InsP$_7$ were based on a previously described method.[37] A 1 X reaction buffer containing 30 mM HEPES at pH 7.2, 50 mM NaCl, 6 mM $MgSO_4$, and 1 mM DTT was prepared. To this reaction buffer, 0.3 mM InsP$_6$ (phytic acid solution [Sigma-Aldrich 593,648]) and 5 mM ATP (Mg salt [Sigma-Aldrich A9187]) were added as substrates. For the generation of 5-InsP$_7$, the auxiliary reaction for the ATP recycles is required. In the reaction mixture, 25 U/mL creatine phosphokinase (CPK [Sigma-Aldrich C3755]) catalyzed the transfer of the phosphate group from phosphocreatine (6 mM) to the ADP generated by Ip6k1 to regenerate ATP. As recommended, CPK was prepared in 0.25 M glycylglycine (pH 7.4). To trigger the reaction, 10 μg GST-Ip6k1 was added to the reaction mixture. The reaction volume was adjusted to 50 μL with ddH_2O, and after a brief spin, the mixture was incubated at 37°C overnight with rotation. A large vertical protein electrophoresis system (24 cm long × 12 cm wide × 1.5 mm height) was used for the isolation of 5-InsP$_7$. The 35.5% (w/v) gel was prepared using the following: 0.05% (w/v) ammonium persulfate, 0.05% (w/v) TEMED, 1X TBE buffer, andacrylamide:bis-acrylamide (19:1). The gel was pre-run using 1X TBE at 4°C for 30 min at 200 V. The samples containing 1 X Orange G dye were loaded into individual wells, and the gel was run using pre-chilled TBE for approximately 16–18 h at 7 mA/gel and 4°C. The gel was stained with toluidine blue buffer (0.1% [w/v] toluidine blue, 20% [w/v] methanol, and 2% [w/v] glycerol) for 5 min and subsequently transferred to a destaining solution containing 50% (w/v) methanol and 10% (v/v) glycerol. The 5-InsP$_7$ gel band was eluted and placed in a tube and washed with 10 mL ddH_2O before the extraction. Dehydration-hydration cycles were used for the extraction of 5-InsP$_7$. First, the gel was transferred to a fresh tube with 5 mL of 50% (w/v) methanol and rotated at 40 rpm and 25°C for 2 h. The gel was then transferred to a new tube with 5 mL of ddH_2O and briefly spun for 2 h. This dehydration-hydration cycle was repeated twice. Further, 5-InsP$_7$ was concentrated by evaporating methanol and ddH_2O from the sample by heating in SpeedVac at 55°C. The sample was centrifuged for 2 min at 2,400 *g* and 25°C to separate acrylamide particles, and the supernatant was transferred to a new tube. The 5-InsP$_7$ was stored at 4°C until further analysis.

Identification and quantification of 5-InsP$_7$ using LC-MS

5-InsP$_7$ was identified and quantified using BRUKER Co. with LC (Bruker Elute) with a Waters Hillic (1.7 μm, 100 × 2.1 mm) column using 10% mobile phase A (H_2O with 5 mM ammonium acetate) and 90% mobile phase B (CH_3CN with 5 mM ammonium acetate) at a flow rate of 0.4 mL/min for 5 min. The electrospray ionization was set to the negative mode, and the scan mode was set to 50–1,300 *m/z*. Sodium formate cluster ions were used as the external standard for calibration. The capillary voltage was set to 3,000 V (-ESI). The pressure of the nebulizer gas (nitrogen) was 1.80 bar, the flow rate of the dry gas was 8.0 mL/min, and the dry temperature was set to 220°C. Finally, the acquisition mode of the fragment ions was set to the scan mode. InsP$_6$ was diluted with 50% (v/v) methanol to a concentration of 1.432 ppm for the standard.

Purification of inositol phosphates by titanium dioxide pull-down

The extraction of inositol phosphates was performed according to a previous method.[74] The *S. cerevisiae* strain CEN.PK 113-11C and QL5 strain with and without the *OCA5* deletion were grown in synthetic complete medium (SCM) overnight with shaking at 30 °C to logarithmic phase with OD_{600} around 2. The medium was centrifuged at 10,000 *g* for 5 min at 4°C to harvest the cells. Pellets were washed once by ddH_2O and resuspended in 500 μL of 1 M perchloric acid solution (1 M perchloric acid, 5 mM EDTA). The mixture was vigorously vortexed for 5 min at 4 °C with 300 μL of acid-washed glass beads (Sigma Aldrich), followed by centrifuging at 15,000 *g* for 5 min at 4°C to remove the fragment. All the buffers were pre-chilled to 4°C. The TiO_2 beads (Titansphere TiO_2 5 μm; GL Sciences) were prepared as reported,[75] pre-washed by perchloric acid solution, and resuspended in 50 μL of perchloric acid solution. The supernatant was incubated with the TiO_2 for 15–20 min with a brief spin at 4°C. Then, the mix was centrifuged at 3,500 *g* for 1 min at 4°C to harvest the TiO_2 beads which were washed with 500 μL of 1 M perchloric acid solution once. After that, these beads were resuspended by 200 μL of 2.8% ammonium hydroxide and incubated for 5 min with a brief spin twice. 400 μL aliquots were concentrated by using a SpeedVac evaporator for 1–3 h at 40 °C or 60 °C to remove ammonia.

In vivo analysis of InsPs by CE-ESI-MS

Quantification of inositol polyphosphate was performed by CE-ESI-MS (QQQ) with sufficient sensitivity to profile 1,5-InsP$_8$, 5-InsP$_7$, 1-InsP$_7$, InsP$_6$ in yeast.[76] CE-ESI-MS analysis was performed on an Agilent CE 7100 system interfaced with a triple-quadrupole tandem MS Agilent 6495c system, by an Agilent Jet Stream ESI source and sheath liquid coaxial interface. An Agilent 1200 isocratic LC pump was employed to constantly deliver a slow sheath liquid flow via a splitter set with a ratio of 1:100. All experiments were performed with a bare fused silica capillary with a length of 100 cm and 50 μm internal diameter. 35 mM ammonium acetate titrated by ammonia solution to pH 9.7 was used as background electrolyte. The sheath liquid composed of a water–isopropanol (1:1) mixture was introduced at a flow rate of 10 μL/min. Capillary was flushed with background electrolyte by 400 s between runs. Samples were injected by applying 100 mbar pressure for 15 s (30 nL). CE separation voltage was +30 kV. The MS source parameters setting were as follows: nebulizer pressure was 8 psi, gas temperature was 150°C and with a flow of 11 L/min, sheath gas temperature was 175°C and with a flow at 8 L/min, the capillary voltage was −2,000 V with nozzle voltage 2,000 V. Negative high-pressure RF and low-pressure RF (ion funnel parameters) were 70 V and 40 V, respectively. Mass spectrometer parameters for multiple reaction monitoring (MRM) transitions are shown in Table S5.

Inositol polyphosphates extracts were dissolved in 120 μL water. Internal standard (IS) stock solutions of 3.4 μM [$^{13}C_6$]1,5-InsP$_8$, 10.0 μM [$^{13}C_6$]5-InsP$_7$, 11.8 μM [$^{13}C_6$]1-InsP$_7$, 176 μM [$^{13}C_6$]InsP$_6$, and 1880 μM [$^{13}C_{10}$]ATP were used for the spiking experiments; 1 μL of IS stock solution was mixed into 20 μL samples. 0.17 μM [$^{13}C_6$]1,5-InsP$_8$, 0.50 μM [$^{13}C_6$]5-InsP$_7$, 0.59 μM [$^{13}C_6$]1-InsP$_7$, 8.8 μM [$^{13}C_6$]InsP$_6$, and 94 μM [$^{13}C_{10}$]ATP were the final concentrations inside samples. Quantification of 1,5-InsP$_8$, 5-InsP$_7$, 1-InsP$_7$, InsP$_6$, and ATP was performed with known amounts of corresponding heavy isotopic references spiked into the samples. ^{13}C labeled inositol references were kindly provided by Dorothea Fiedler (FMP, Berlin).[77]

Oca5 activity assay

The activity of Oca5 was assayed as previously mentioned in previous report[35] with slight modifications. The reaction mixture contained 30 mM HEPES (pH 7.3), 50 mM NaCl, 6 mM $MgSO_4$, and 1 mM DTT. To this mixture, 30 mM generated 5-InsP$_7$, quantified by comparison with InsP$_6$[37], was added as the substrate. The purified enzyme, 8 μg GST-Oca3 (+) or water (−), and 40 μg GST-Oca5 (+) or water (−) was added to trigger the reaction. The concentration of the reaction product was analyzed using PAGE as described above.

Flow cytometric analysis for MitoTracker green staining of mitochondria

For flow cytometric analysis, the strain was cultured in a flask with defined minimal medium using either 20 g/L glucose or ethanol as the carbon source. The culture conditions were the same as previously described. Exponential-phase samples were used for the analysis, which were obtained when the OD_{600} was approximately 0.6 for glucose-supplemented media and 0.8 for ethanol-supplemented media. The culture was diluted to OD_{600} 0.2 using PBS buffer supplemented with 25 mM glucose or 20 g/L ethanol (as applicable) and was stained with MitoTracker Green (MTG) FM to a final concentration of 100 nM for 30 min at room temperature in the dark and with gentle rotation. Subsequently, the sample was directed for flow cytometric analysis.

MTG staining of the mitochondria of *P. pastoris* X-33 and the *P. pastoris oca5*Δ strain was performed. Under nitrogen limitation, *P. pastoris* mate and form diploid cells. Therefore, to maintain them in the haploid state, the medium was changed to YPD, and the staining for MTG was performed as recommended.[78] Similar to *S. cerevisiae*, the samples at exponential phase were used for analysis, when the OD_{600} was approximately 0.6. The strain was diluted to OD_{600} 0.2 by adding YPD medium and stained for 30 min with MTG to a final concentration of 100 nM at room temperature in the dark with gentle rotation. Thereafter, the samples were washed with PBS buffer and resuspended in PBS buffer for flow cytometric analysis.

Isotope labeling

The minimal medium with 20 g/L 100% D-Glucose-1-^{13}C (Sigma-Aldrich) in a shake flask was used for the sample preparation for the isotope labeling experiment. Strains were inoculated with OD_{600} 0.01 and harvested in the mid-to late-exponential phase (OD_{600} around 2).

The quench and extraction methods were followed as previously described[79] with slight modifications. For quenching, 3 mL medium was transferred immediately into the 50 mL tube with 30 mL pure methanol (precooling in −80°C fridge) and vortexed around 1 s. Cells were collected using a vacuum filtration system with a 0.8 μm pore size filter membrane. 10 mL precooling pure methanol was used to wash the cells to prevent the isotope labeling medium residue. The filter membrane with the cells was transferred into a new 50 mL tube with 15 mL 75% (v/v) ethanol (preheated in a water bath at 75°C). Quickly vortex the tube to make sure the filter membrane submerges in the ethanol. The tube was incubated in a water bath at 95°C for 3 min for the extraction. Then the tube was placed on the ice to cool. The vacuum filtration with a 0.8 μm pore size filter membrane was used to remove the major cell debris to collect the supernatant. The supernatant was evaporated in SpeedVac at 4°C and the volume of the supernatant was concentrated to less than 1 mL. Before the MS analysis, the sample was filtrated with a 0.22 μm pore size filter membrane. 20 μL sample was used for the UPLC-MS analysis. If not specifically mentioned, the tube was placed on the ice. The isotopic labels of metabolites were determined with UPLC-MS/MS (SCIEX TRIPLETOF 6600). The metabolic samples were separated by a ZIC-HILIC column (100 mm × 2.1 mm, 3.5 μm) (Merck, German). Solvents were composed of water/acetonitrile/ammonium acetate (A: 100%/0%/10mM, B: 0%/100%/0mM). The LC method was 0–3 min (90% B), 3–25 min (90%–60% B), 25–30 min (60% B), 30–38 min (90%B). A flow rate of 0.3 mL/min was employed.

Microscopy imaging

Fluorescence microscopy images were captured as previously mentioned.[45] SC-ura medium supplemented with 20 g/L glucose was used for the culture of yeast. The yeast strains expressing the corresponding plasmids were incubated in a shaker incubator at 200 rpm and 30°C until OD_{600} was approximately 0.6 (early log phase). The sample was pipetted onto poly-L-lysine-coated slides with the remaining suspension immediately withdrawn through aspiration. Subsequently, 1 μL 4′,6-diamidino-2-phenylindole (DAPI) stain (2.5 g/mL DAPI in 80% glycerol) was pipetted onto the sample, and the slide was covered with a coverslip. Sequential scans were performed for GFP and DAPI to avoid their spectral overlap. Octuplicate biological independent experiments were performed for this assay.

QUANTIFICATION AND STATISTICAL ANALYSIS

The significant comparisons of two different groups are indicated in the graphs statistical analysis was performed using two-tailed unpaired Student's t test (*$p < 0.05$, **$p < 0.01$, ***$p < 0.001$). The graphs represented means ± SD unless otherwise indicated, as described in the figure legends. Data were processed in Excel. The adjusted p-values calculated using the Benjamini-Hochberg method[80] and $\log_2$ fold change of the differential gene expression analysis were used as the inputs for enrichment analysis. The Wilcoxon rank-sum test was used to evaluate the p value for each reaction in the FVA analysis.

Supplemental figures

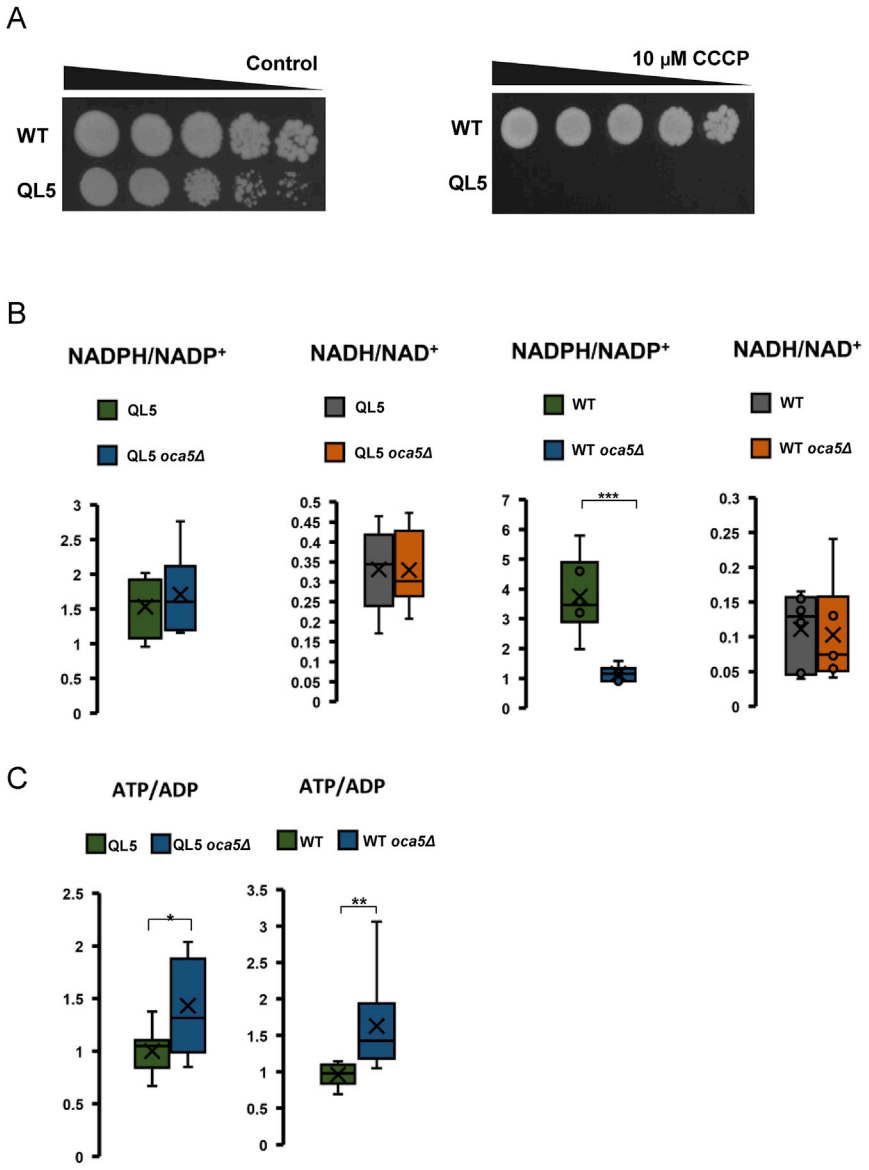

Figure S1. The energy and cofactor measurements of the QL5 strain and *OCA5* deletion strain, related to Figures 1 and 3

(A) CCCP could inhibit the growth of the QL5 strain. Strains were pre-cultured in the minimal medium consisting of 20 g/L glucose and then spotted on the plate without and with CCCP. (B) Ratio of NADPH/NADP$^+$ and NADH/NAD$^+$ of *oca5*Δ in QL5 (first and second) and WT (third and fourth). (C) ATP/ADP ratio of *oca5*Δ in the QL5 (left) and WT (right) strain. The mean ± SD was based on biological triplicates. Statistical analysis was performed using two-tailed Student's t test (*$p < 0.05$, **$p < 0.01$, ***$p < 0.001$).

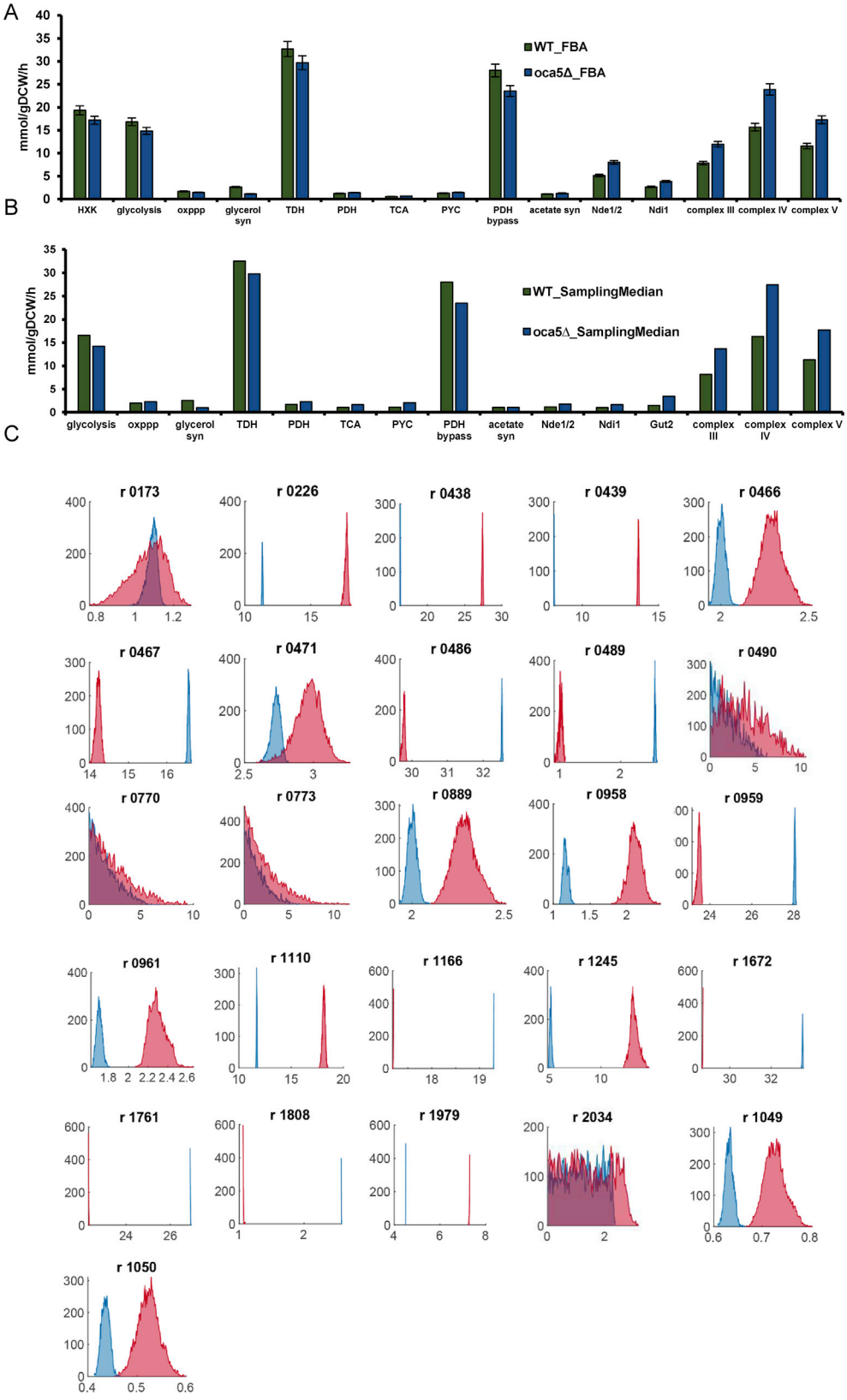

(legend on next page)

Figure S2. The absolute flux and the flux sampling of WT and oca5Δ strains, related to Figure 3

(A) The absolute metabolic fluxes in FBA of the key nodes in central carbon metabolism of WT (green bars) and *oca5*Δ (blue bars) were performed using the yeast model Yeast849 as reported50. Samples for metabolite measurements were taken in minimal medium during the exponential phase of batch fermentation. (B) The flux sampling median of the key nodes in central carbon metabolism of WT (green bars) and *oca5*Δ (blue bars). The p value shown in Table S1. (C)Flux (x axis) and number of samples (y axis) of representative reactions (Table S1) of WT (blue) and oca5Δ (red) in flux sampling. The error bars represent 95% confidence intervals of flux estimates. Abbreviations of nodes and reactions were defined in Table S1.

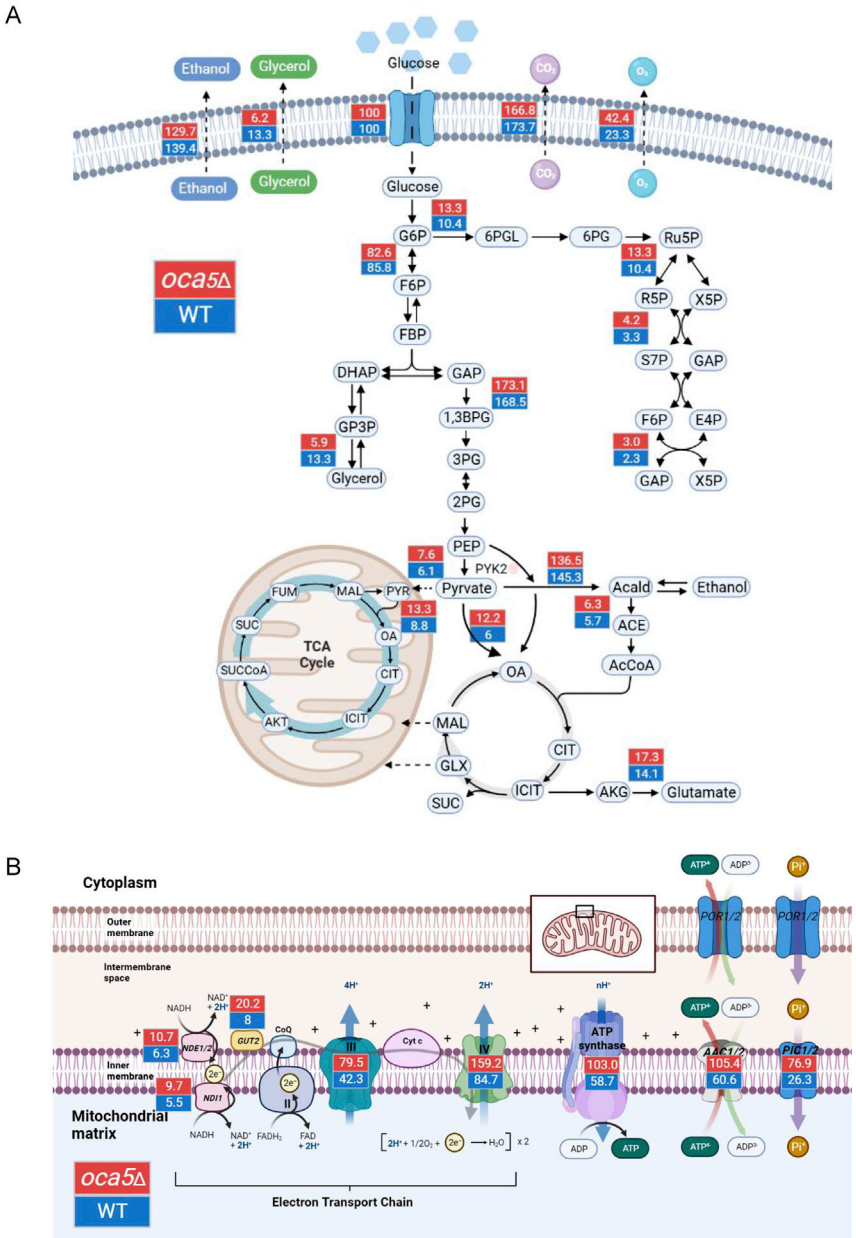

Figure S3. The flux sampling of WT and *oca5Δ* in the pathway, related to Figure 3

The number in the key step of glycolysis (A) and the respiratory chain (B) was the median in flux sampling.

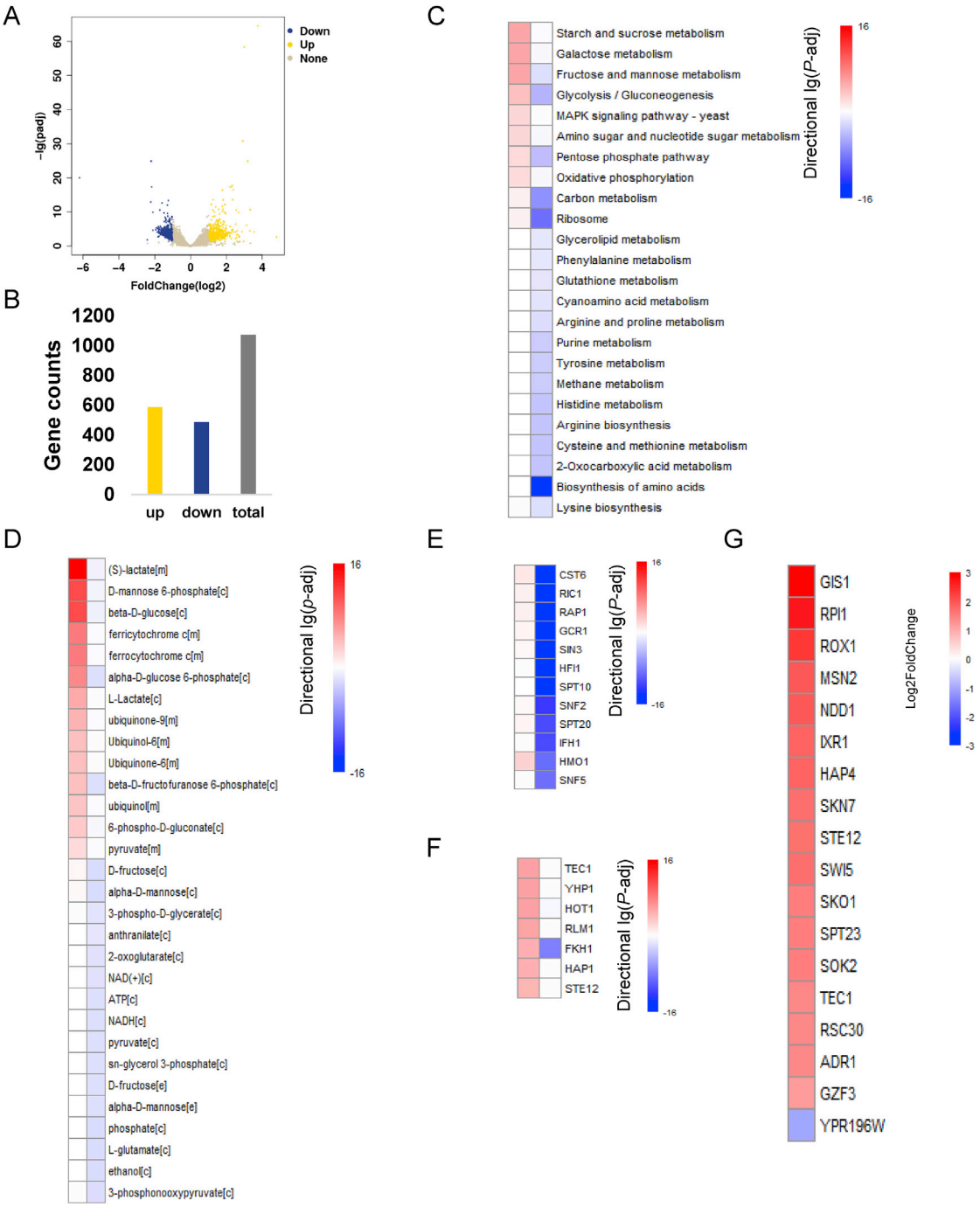

Figure S4. The transcription profiling of the *oca5*Δ strain, related to Figures 3 and 7

(A and B) The summary of significantly regulated genes (P-adj value <0.05) in *oca5*Δ compared with WT. Significantly upregulated (Log2 fold change >1) genes are shown in yellow and significantly downregulated (Log2 fold change < −1) genes are shown in blue. (C and D) The pathway enrichment analysis and the metabolite enrichment analysis of mix-directional up class (red) and mix-directional down class (blue) genes (P-adj <0.05). (E and F) The top five value enriched TFs scored by the modulation in expression level of genes that were controlled by TFs in mix-directional down class (blue) and mix-directional up class (red). The log(P-adj) value was given to 16 (up) or −16 (down) if the absolute value of these P-adj less than10–16. (G) The intersection of the TFs which were scored by the modulation in expression level of genes that controlled by TFs in distinct-directional up class (P-adj <0.05) with the expression significantly changed (Log2 fold change >1 or < −1 and P-adj <0.005).

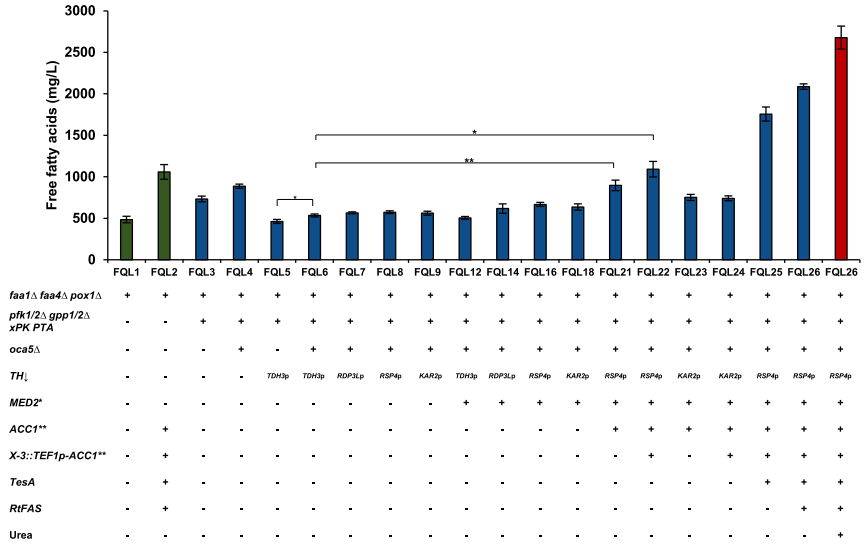

Figure S5. Hybrid-glycolysis yeast for FFAs production, related to Figure 4

The deletion of two main fatty acyl-CoA synthetase encoding genes *FAA1* and *FAA4* and the deletion of the fatty acyl-CoA oxidase *POX1* prevent the degradation of FFAs by β-oxidation could realize the basal production of FFAs in WT and hybrid-glycolysis yeast. Since the FFAs production requires NADPH as the reducing factor, and the *TH* with the *TDH3* promoter may be too strong thus transforming too much NADPH to NADH and may restrict FFAs production in QL5, the *TDH3* promoter of *TH* was replaced to *RPL3*p, *RPS4A*p, and *KAR2*p, respectively. Yeast promoter strength values in glucose lacking amino acids medium[81] were 40%, 20%, and 10% to *TDH3*p, respectively. The sequence for each promoter is listed in Table S3. Meanwhile, to further decrease fermentation, *MED2** with a stop codon432Y in a tail module of RNA polymerase II mediator, which led to decreased fermentation in yeast,[17] was introduced. Moreover, the two mutations, namely, S659A and S1157A, were introduced into native *ACC1*.[82] Another copy of *ACC1*** expressed under the *TEF1* promoter activity was integrated into the chromosome. The truncated *E. coli* thioesterase *TesA* and the *Rhodosporidium toruloides FAS* (*RtFAS1* and *RtFAS2*) were overexpressed.[30] The FFAs were produced by the hybrid-glycolysis yeast in shake flasks at 200 rpm and 30°C until the fermentation was completed. The minimal medium contained 20 g/L glucose as a carbon source and 7.5 g/L $(NH_4)_2SO_4$ as a nitrogen source. For the optimization of the culture process, the nitrogen source, $(NH_4)_2SO_4$, in the minimal medium was changed to 2.27 g/L urea as reported.[31] Statistical analysis was performed using two-tailed Student's *t* test (*$p < 0.05$, **$p < 0.01$, ***$p < 0.001$). All data are presented as mean ± SD of biological triplicates.

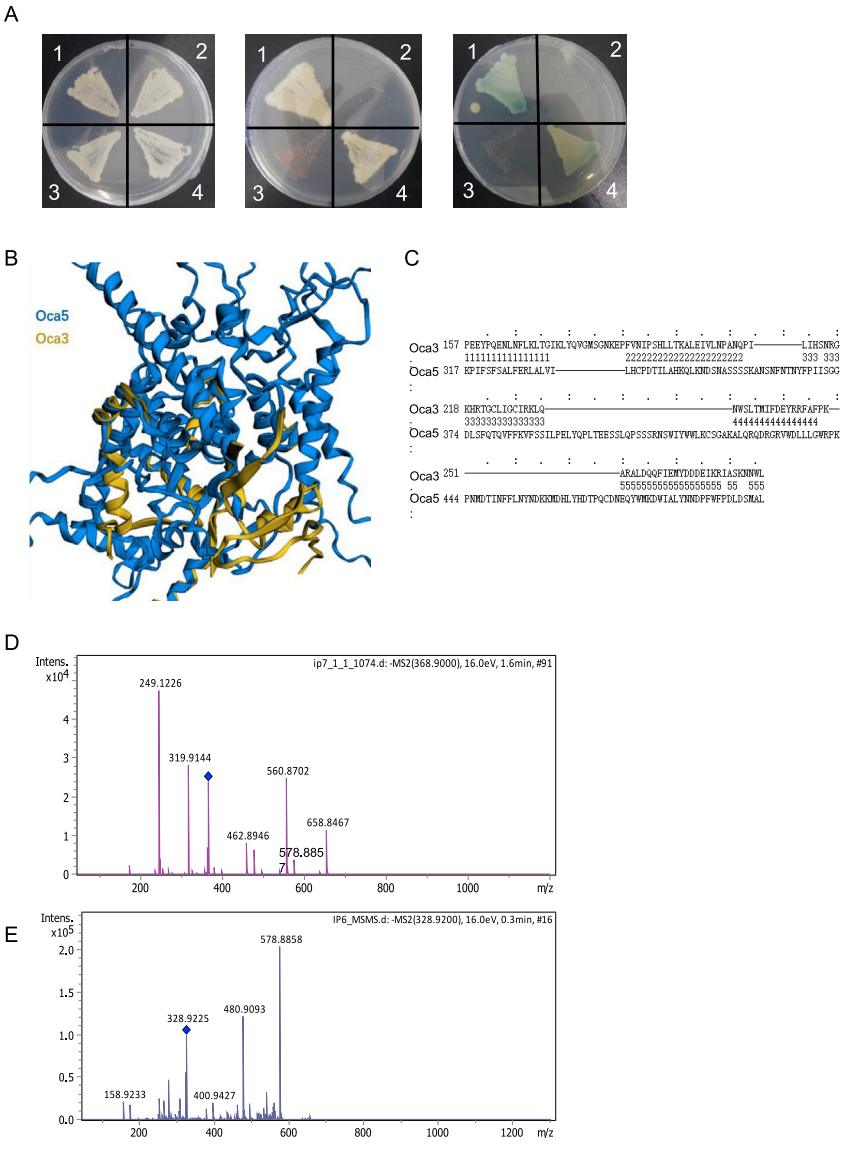

Figure S6. The Oca5 was an inositol pyrophosphatase, related to Figure 5

(A) Interaction test of Oca5 and Oca3 by yeast two-hybrid analysis. The Matchmaker Gold Yeast Two-Hybrid System was used for the analysis. The result presented the growth of yeast cells expressing binding domain (BD) and active domain (AD) fused with Oca3 and Oca5, respectively. (left): Yeast growth on the DDO plate showing successful co-transformations. (middle): Yeast growth on the selective QDO plate. (right): Yeast growth on the selective QDO/X/A plate. These results indicated that there was no significant protein-protein interaction between Oca3 and Oca5. (1) pGADT7-T together with pGBKT7-53 as the positive control; (2) pGADT7-T together with pGBKT7-Lam as negative control; (3) pGBKT7-Oca3 together with pGADT7-Oca5; (4) pGBKT7-Oca5 together with pGADT7-Oca3. The superimposed structure of Oca5 and Oca3 (B and C). The structure of Oca3 was from *S. cerevisiae* (PDB: 6E3B).[83] The structure of Oca5 was from AlphaFold Protein Structure Database (https://alphafold.ebi.ac.uk/). FATCAT was used to compare the structure of these two proteins (https://fatcat.godziklab.org). Chain 1 and chain 2 represented Oca3 and Oca5. Amino acid positions were from PDB and the numbers between alignments were block index. Five blocks were found with RMSD score 1.81, 1.11, 0.91, 1.63 and 3.75, respectively. RMSD score 3 was recognized as a threshold for similar structures. (D) The peak at *m/z* 658.8462 was 5-InsP$_7$ loss of H_2PO_4 fragment; the peak at *m/z* 578.8857 was the ion 658.8462 (*m/z*) loss of H_2PO_3 fragment; the peak at *m/z* 560.8706 was the ion 578.8857 (*m/z*) loss of H_2O fragment. (E) The peak at *m/z* 578.8858 was InsP$_6$ loss of H_2PO_3 fragment; the peak at *m/z* 480.9093 was the ion 578.8858 (*m/z*) loss of H_2PO_4 fragment.

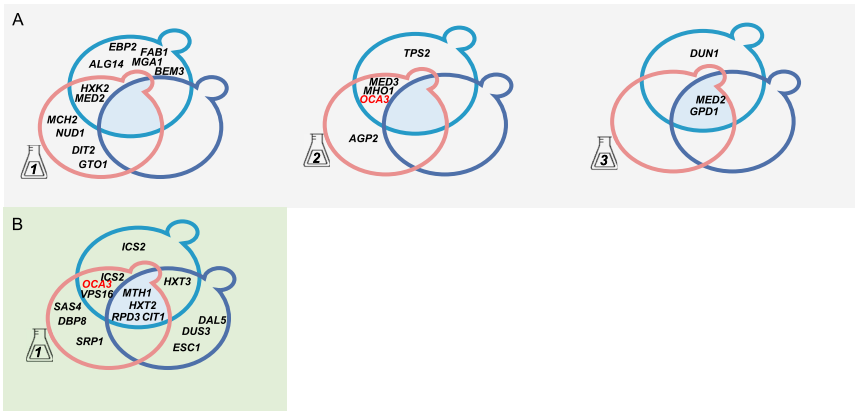

Figure S7. Inositol pyrophosphate mutations were reported in Crabtree-negative yeasts, related to Figure 5

The Venn diagram of the genome sequencing result from similar research (Dai et al.[17] shown as A and Zhang et al.[23] shown as B). The intersection of each flask indicated the dominant mutations of each parallel line